



## Research paper

Mode of action of *p*-quinone derivatives with trypanocidal activity studied by experimental and *in silico* models

Andres Ballesteros-Casallas<sup>a,b,1</sup>, Cristina Quiroga<sup>c,1</sup>, Cecilia Ortiz<sup>c</sup>, Diego Benítez<sup>c</sup>, Pablo A. Denis<sup>d</sup>, David Figueroa<sup>a</sup>, Cristian O. Salas<sup>e</sup>, Jeanluc Bertrand<sup>e</sup>, Ricardo A. Tapia<sup>e</sup>, Patricio Sánchez<sup>e</sup>, Gian Pietro Mischione<sup>a,\*</sup>, Marcelo A. Comini<sup>c,\*\*</sup>, Margot Paulino<sup>b,\*\*\*</sup>

<sup>a</sup> COBO, Computational Bio-Organic Chemistry, Chemistry Department, Universidad de Los Andes, Carrera 1 18A-12, Bogotá, 111711, Colombia

<sup>b</sup> Bioinformatics Center, DETEMA Department, Faculty of Chemistry, Universidad de la Repùblica, General Flores 2124, Montevideo, 11600, Uruguay

<sup>c</sup> Laboratory Redox Biology of Trypanosomes, Institut Pasteur de Montevideo, Mataojo 2020, Montevideo, 11400, Uruguay

<sup>d</sup> Computational Nanotechnology, DETEMA Department, Faculty of Chemistry, Universidad de la Repùblica, General Flores 2124, Montevideo, 11600, Uruguay

<sup>e</sup> Departamento de Química Orgánica, Facultad de Química y de Farmacia, Pontificia Universidad Católica de Chile, Av. Vicuña Mackenna 4860, Santiago, 6094411, Chile

## ARTICLE INFO

## ABSTRACT

## Keywords:

Genetically-encoded redox biosensor

*Leishmania*

*p*-Quinones

QSAR

Redox cycling

Thiol-redox balance

*Trypanosoma*

Quinones are attractive pharmacological scaffolds for developing new agents for the treatment of different transmissible and non-transmissible human diseases due to their capacity to alter the cell redox homeostasis.

The bioactivity and potential mode of action of 19 *p*-quinone derivatives fused to different aromatic rings (carbo or heterocycles) and harboring distinct substituents were investigated in infective *Trypanosoma brucei brucei*. All the compounds, except for a furanequinone ( $EC_{50}=38\ \mu M$ ), proved to be similarly or even more potent ( $EC_{50} = 0.5-5.5\ \mu M$ ) than the clinical drug nifurtimox ( $EC_{50} = 5.3\ \mu M$ ). Three furanequinones and one thiazolequinone displayed a higher selectivity than nifurtimox. Two of these selective hits resulted potent inhibitors of *T. cruzi* proliferation ( $EC_{50}=0.8-1.1\ \mu M$ ) but proved inactive against *Leishmania infantum* amastigotes.

Most of the *p*-quinones induced a rapid and marked intracellular oxidation in *T. b. brucei*. DFT calculations on the oxidized quinone (Q), semiquinone ( $Q^\bullet$ ) and hydroquinone ( $QH_2$ ) suggest that all quinones have negative  $\Delta G$  for the formation of  $Q^\bullet$ . Qualitative and quantitative structure-activity relationship analyses in two or three dimensions of different electronic and biophysical descriptors of quinones and their corresponding bioactivities (killing potency and oxidative capacity) were performed.

Charge distribution over the quinone ring carbons of Q and  $Q^\bullet$  and the frontier orbitals energies of SUMO ( $Q^\bullet$ ) and LUMO (Q) correlate with their oxidative and trypanocidal activity. QSAR analysis also highlighted that both bromine substitution in the *p*-quinone ring and a bulky phenyl group attached to the furane and thiazole rings (which generates a negative charge due to the  $\pi$  electron system polarized by the nearby heteroatoms) are favorable for activity.

By combining experimental and *in silico* procedures, this study disclosed important information about *p*-quinones that may help to rationally tune their electronic properties and biological activities.

## 1. Introduction

Quinones are chemical scaffolds present in many natural compounds that serve important functions in biology due to their redox properties in living organisms [1,2]. The *para*-ketone groups confer to these

molecules a high susceptibility for undergoing enzyme-catalysed one-electron and two-electron reductions that, under certain conditions, can be fully reversible. This feature makes quinones versatile redox cofactors for important metabolic processes that involve electron transport [3]. In addition, the redox reaction of *p*-quinones involves the

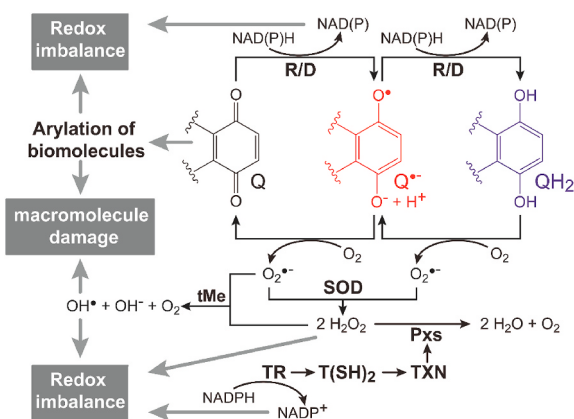
\* Corresponding author

\*\* Corresponding author.

\*\*\* Corresponding author.

E-mail addresses: [gp.mischione57@uniandes.edu.co](mailto:gp.mischione57@uniandes.edu.co) (G.P. Mischione), [mcomini@pasteur.edu.u](mailto:mcomini@pasteur.edu.u) (M.A. Comini), [margot@fq.edu.u](mailto:margot@fq.edu.u) (M. Paulino).

<sup>1</sup> Both authors contributed equally.



**Scheme 1.** Proposed mechanism of action and redox behavior of *p*-quinones in biological systems. Q: quinone, Q<sup>•</sup>: semiquinone radical, QH<sub>2</sub>: hydroquinone, R/D: NAD(P)H-dependent reductases (R) and dehydrogenases (D), SOD: superoxide dismutase, tME: transition metal. Trypanosomatids lack catalase and hydrogen peroxide (H<sub>2</sub>O<sub>2</sub>) is decomposed by different types of peroxidases (Pxs) that are trypanolectin (TXN)-dependent. The disulphide reductase TXN receives electrons from dihydro-trypanothione (T(SH)<sub>2</sub>), which is kept in reduced state by the NADPH-dependent enzyme trypanothione reductase (TR).

generation of reactive oxygen species (ROS) and the consumption of reducing equivalents (NAD(P)H and low molecular weight thiols) as shown in Scheme 1. The superoxide radical anion (O<sub>2</sub><sup>•</sup>), semi-quinone radical and hydrogen peroxide as well as the depletion of the cellular reducing power can produce oxidative stress [4], and have been proposed as key redox species of the mechanism of action of antitumoral and antiparasitic compounds [5–8].

Based on their redox properties, several natural and synthetic derivatives of quinones have been studied as potential chemotherapy drugs for infectious diseases caused by protozoan parasites such as Human African Trypanosomiasis (HAT, also known as sleeping sickness), Chagas disease and leishmaniasis, which are considered neglected diseases according to the World Health Organization (WHO) [6,9,10]. Due to globalization and migrations, these diseases spread to non-endemic locations, such as the United States of America, Japan and Europe, increasing the risk of infection and potential cases worldwide [11]. HAT is endemic in sub-Saharan African countries and among the species infecting mammals is *Trypanosoma brucei brucei* [12]. Chagas disease, is caused by *Trypanosoma cruzi* and affects millions of people, mainly in Central and South American countries [13]. Leishmaniasis is endemic in 88 countries, with an estimated of 700,000 to 1 million new cases occurring each year [11].

Current drugs used against HAT, American trypanosomiasis and leishmaniases, dating back to the early 20th century, have several side effects, low efficacy and are excessively toxic [14], therefore, the development of new drugs is important to improve these aspects and to overcome the development of resistance [9,15]. In this context, compounds derived from natural naphthoquinones have long been considered as privileged scaffolds in the development of agents with antiparasitic activity because in traditional medicine, plants containing them have been used for the treatment parasitic infections [16,17].

Among the natural *p*-quinone derivatives that have been extensively studied are lapachol (I, Fig. 1) and α-lapachone (II, Fig. 1), extracted from lapacho tree, which have shown interesting trypanosomicidal and leishmanicidal activity [10,18–20]. Several research groups have reported the synthesis and the antiparasitic evaluation of new derivatives of these natural products, such as, 2-aryloxy-naphthoquinones and 2-amino naphthoquinones (III and IV, Fig. 1) [21,22]. Structure-activity relationship (SAR) studies showed that the aryloxy or phenylamino fragments enhance the antiparasitic activities [22–25].

In view of the electrochemical features of *p*-quinones making them potent pro-oxidant molecules in biological systems and the experimental evidence suggesting that quinones can inhibit enzymes of the redox metabolism [26–29], in this work we decided to investigate the bioactivity against trypanosomatids of a set of 19 quinones, which can be divided into two subsets. The former corresponds to a small group of 2-aryloxy-naphthoquinones (Fig. 2, Series I) [30], while the latter (Fig. 2, Series II–IV) includes phenoxy- and phenylamino scaffolds [31]. First, we investigated the bioactivity and intracellular oxidant capacity of these quinones against the bloodstream form of *T. b. brucei* as well as their cytotoxicity on murine macrophages (J774 cells). The most selective quinones were investigated for their capacity to affect the viability of *T. cruzi* infecting the cytosol of primate epithelial cells and of *L. infantum* residing in the phagolysosome of macrophages. A detailed *in silico* analysis was performed with the aim to identify and characterize the molecular descriptors associated with quinones bioactivity. DFT investigation was carried out to obtain information about the physico-chemical properties of these quinones considering all redox, parasitological and reactivity indexes, which were put together to perform structure-activity relationship (SAR), 2D-QSAR and 3D-QSAR analysis.

## 2. Results and discussion

### 2.1. Quinones activity against the infective stage of different trypanosomatids

The killing potency of the *p*-quinones (Fig. 2) against the highly proliferating and blood circulating stage of *T. b. brucei* was tested using a bioluminescence assay that reports parasite number and viability [32]. The parasites were treated for 24 h with the compounds and control.

Except for the halogenated furanequinone 7 (EC<sub>50</sub> = 38 μM), all compounds exerted a potent anti-*T. b. brucei* activity with EC<sub>50</sub> values similar or lower (EC<sub>50</sub> range 0.5–5.5 μM; Table 1) than the reference drug nifurtimox (EC<sub>50</sub> = 5.3 μM), which, in combination with eflornithine, is used to treat the chronic stage of HTA [33].

All naphtho (Series I) and oxazolequinones (Series IV) analogues presented similar anti-trypanosomal activity (EC<sub>50</sub> range 1.6–5.5 μM). This suggests that none of the different substituents added to the naphthoquinones and oxazolequinones contributes to the biological activity against *T. brucei* with respect to the parental structural scaffold, namely 4 or 5 and 16, respectively.

In contrast, the activity of the furane- and thiazole-derivatives (Series II and III) showed a more scattered behavior with cytotoxic potencies that differed one order of magnitude between analogues (Series II: EC<sub>50</sub> range 0.9–38 μM, and Series III: EC<sub>50</sub> range 0.5–5 μM).

For Series II, the less active analogue proved to be the brominated furanequinone 7 (EC<sub>50</sub> = 38 μM). Interestingly, addition of an aniline

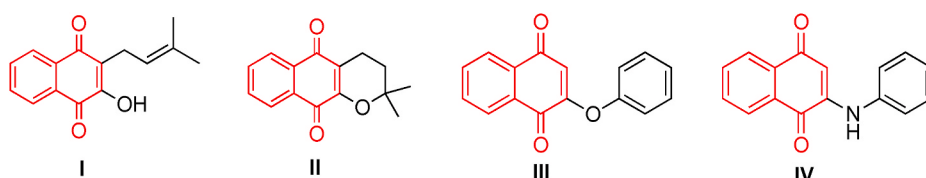


**Fig. 1.** Chemical structures of well-known *p*-quinone derivatives with antiparasitic activity.

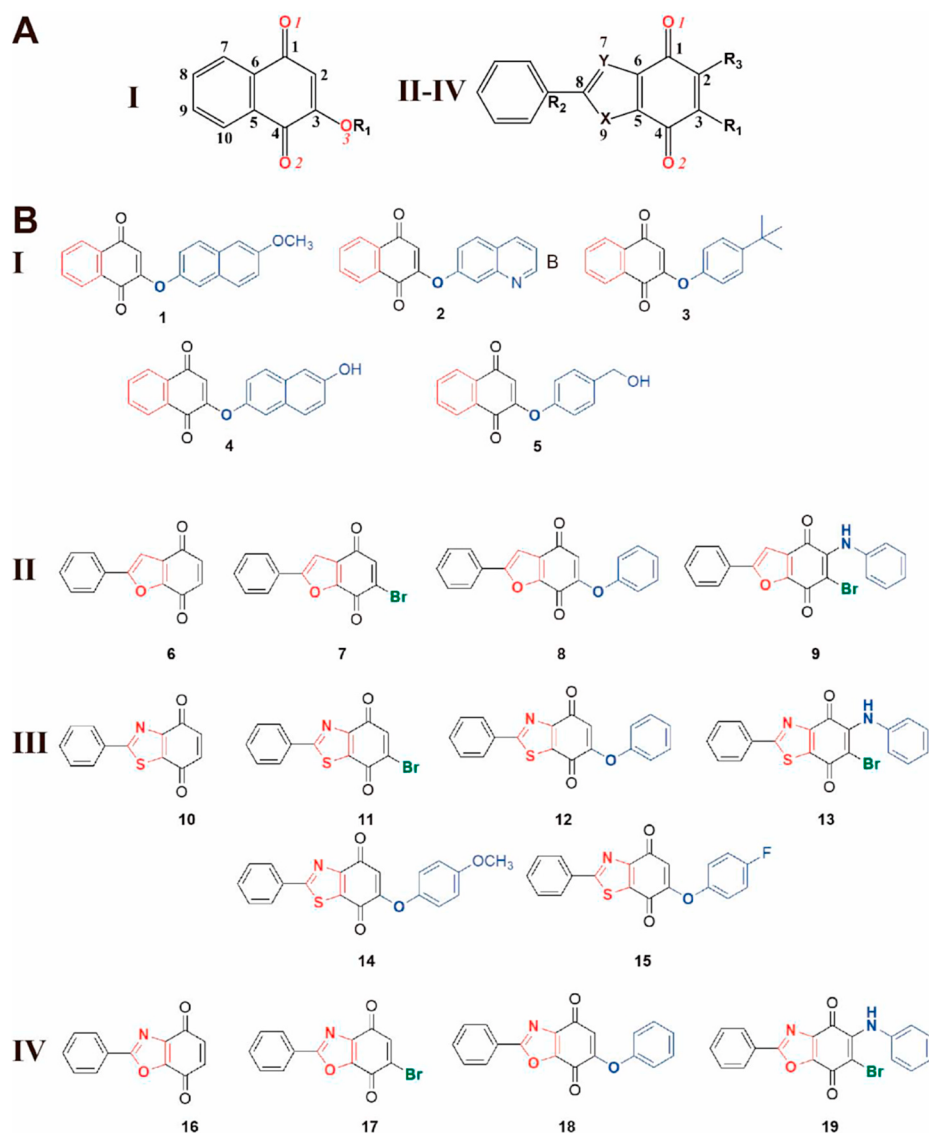


**Fig. 2. Structure of *p*-quinones selected for biological and *in silico* studies. A)** Major *p*-quinones scaffolds (Series indicated in Roman numbers) with atoms labeled according to the numeration used for the putative charge descriptors. Oxygen atoms (in red) are re/numerated. Y and X denote the heterocycle arrangement (N, O, S or C atoms). **B)** The compounds are grouped according to the chemical nature of the quinone moiety as Series I (naphtho), II (furane), III (thiazole) and IV (oxazole).

fragment to 7 increased by 40-folds the activity of the analogue (9 EC<sub>50</sub> = 0.9 μM). The unsubstituted quinone (6) or its aryloxy derivative (8) showed a similar 3-fold lower activity than 9 but 13-folds higher than 7, supporting that bromination alone impairs compound bioactivity.

For Series III, notably and like the furane-derivatives, the brominated analogue substituted with an aniline group proved to be the most active analogue of the series (13 EC<sub>50</sub> = 0.5 μM). This suggests a major role of the halogen and aniline combination in compound biological activity. Finally, no significant differences in potency were observed for the remaining analogues 11, 12, 14 and 15 (EC<sub>50</sub> range = 1.5–5.0 μM), which confirms the null additive contribution of mono-substitutions to the activity of the parental thiazolequinone scaffold, namely 10 (EC<sub>50</sub> = 1.3 μM).

With respect to the role of the substituents in the different quinone scaffolds, it is worth noting that the negative effect of the bromination observed for the furanequinone 7 (EC<sub>50</sub> = 38 μM versus EC<sub>50</sub> = 2.6 μM for the unsubstituted 6) was absent when the heterocycle linked to the quinone was a thiazole (11 EC<sub>50</sub> = 1.5 μM) or an oxazole ring (17 EC<sub>50</sub> = 1.6 μM). In fact, both 11 and 17 presented EC<sub>50</sub> values like the

unsubstituted analogues 10 (EC<sub>50</sub> = 1.3 μM) and 16 (EC<sub>50</sub> = 2.3 μM). Regarding the addition of an aniline fragment to the brominated analogues 7, 11 and 17, we observed that it contributed to significantly improve the potency of the furanequinone 9 (EC<sub>50</sub> = 0.9 μM) and to a minor extent that of the thiazolequinone 13 (EC<sub>50</sub> = 0.5 μM) but had a negligible effect on the oxazolequinone 19 (EC<sub>50</sub> = 1.9 μM). Other common substituent included in the analogues of Series II, III and IV was an aryloxy fragment (8, 12, and 18, EC<sub>50</sub> = 2.9, 1.8 and 3.3 μM, respectively), which has a negligible effect in modulating the bioactivity of the quinones as suggested by the similar EC<sub>50</sub> values with their corresponding unsubstituted analogues (6, 10 and 16, EC<sub>50</sub> = 2.7, 1.3 and 2.3 μM, respectively).

## 2.2. Structure-activity relationship (SAR) vs. *T. b. brucei*

In addition to the comparative analysis by pairs presented in the previous section, we carried out a global SAR evaluation to assess quantitatively the role of scaffolds and substituents in *p*-quinone bioactivity. The set of 19 *p*-quinones was subjected to a structural

**Table 1**

Biological activity of *p*-quinones against the infective stages of *T. brucei* (bloodstream form), *L. infantum* and *T. cruzi* (intracellular amastigotes for both parasite species), and murine macrophages (cell line J774). The errors associated to the cell viability determinations differed by less than 15% and are not shown for simplicity.

Series	Compound <sup>a</sup>	<i>T. brucei</i>	Macrophages	<i>T. cruzi</i>	<i>L. infantum</i>
		EC <sub>50</sub> ( $\mu$ M) and SI <sup>b</sup>	CC <sub>50</sub> ( $\mu$ M) and/or % viability	EC <sub>50</sub> ( $\mu$ M) and SI <sup>b</sup>	EC <sub>50</sub> ( $\mu$ M) and SI <sup>b</sup>
<b>I</b>	<b>1</b>	5.2 /~10	~50 (57%) <sup>c</sup>	-	-
	<b>2</b>	3.8 /< 13	< 50 (37%) <sup>c</sup>	-	-
	<b>3</b>	5.5 /< 9	< 50 (24%) <sup>c</sup>	-	-
	<b>4</b>	4.3 / ~14	~50 (63%) <sup>c</sup>	-	-
	<b>5</b>	4.6 / ~11	~50 (49%) <sup>c</sup>	-	-
<b>II</b>	<b>6</b>	2.7 / 44	118	88 % <sup>d</sup>	129 % <sup>d</sup>
	<b>7</b>	38.0 / 2	59	-	-
	<b>8</b>	2.9 / 13	37	-	-
	<b>9</b>	0.9 / 63	57	0.8 / 71	102 % <sup>d</sup>
<b>III</b>	<b>10</b>	1.3 / < 8	< 10 (0%) <sup>d</sup>	-	-
	<b>11</b>	1.5 / 40	61	78 % <sup>d</sup>	91 % <sup>e</sup>
	<b>12</b>	1.8 / < 6	< 10 (40%) <sup>d</sup>	-	-
	<b>13</b>	0.5 / < 22	< 10 (17%) <sup>d</sup>	-	-
	<b>14</b>	1.8 / 43	78	1.1 / 71	90 % <sup>e</sup>
	<b>15</b>	5.0 / < 2	< 10 (5%) <sup>d</sup>	-	-
<b>IV</b>	<b>16</b>	2.3 / < 4	< 10 (21%) <sup>d</sup>	-	-
	<b>17</b>	1.6 / < 6	< 10 (10%) <sup>d</sup>	-	-
	<b>18</b>	3.3 / 14	46	-	-
	<b>19</b>	1.9 / < 5	< 10 (0.5%) <sup>d</sup>	-	-
<b>Nifurtimox</b>		5.3 / 19	100	0.7 / 142	137% (at 20 $\mu$ M)
<b>Benznidazole</b>		-	-	2.2	-
<b>Amphotericin B</b>		-	9.0	-	0.035 / 257
<b>Miltefosine</b>		-	50	-	38.2 / ~1

a Compounds showing low, medium, and high activity against *T. brucei* are highlighted in black, grey and without background, respectively.

b Amastigotes (intracellular stage).

c The selectivity index (SI) is calculated as quotient of the CC<sub>50</sub> macrophage vs. the EC<sub>50</sub> for *T. brucei*, *T. cruzi* or *L. infantum*, respectively.

d The % viability was determined at 50  $\mu$ M compound.

e The % viability was determined at 10  $\mu$ M compound.

f The % viability was determined at 20  $\mu$ M compound.

classification using a SAR strategy and the IC<sub>50</sub> values against infective *T. brucei* reported in Table 1.

Series I is slightly less active than the others and Series III contains a higher number of compounds with low (sub)micromolar anti-*T. brucei* potency (Table 1 and Fig. 2). Given that many substituents at positions R<sub>1</sub>-R<sub>3</sub> are shared between compounds from Series II-IV, it is therefore tempting to generalize that the thiazolequinone scaffold is a chemically privileged structure contributing to compounds' bioactivity.

Notably, the two most potent compounds, **13** (Series III, EC<sub>50</sub> = 0.5  $\mu$ M) and **9** (Series II, EC<sub>50</sub> = 0.9  $\mu$ M), have the same pattern of substituents (R<sub>1</sub> = Br, R<sub>2</sub> = phenyl, R<sub>3</sub> = aniline) and differ only in the nature of the pentane ring (furane for Series II and thiazole for Series III) linked to the quinone moiety. For both series, the aminophenyl

substitution has a clear positive impact on bioactivity. For instance, the derivatives from these series lacking this group in R<sub>3</sub> (**7** and **11**) proved 42- and 3-fold less active than those bearing this substitution (**9** and **13**). In contrast, the contribution of the bromine atom at R<sub>1</sub> appears to depend on the quinone-scaffold context, because its inclusion to a furanequinone was highly detrimental to potency (**7**, EC<sub>50</sub> = 38  $\mu$ M), while its addition to a thiazolequinone did not affect the anti-parasitic activity (**11**, EC<sub>50</sub> = 1.5  $\mu$ M), in both cases when compared to the corresponding unsubstituted analogues (**6**, EC<sub>50</sub> = 2.7  $\mu$ M and **10**, EC<sub>50</sub> = 1.3  $\mu$ M). Interestingly, for the oxazolequinone scaffold, none of the substitutions at positions R<sub>1</sub> and R<sub>3</sub> affected the activity towards *T. brucei*. To determine if this is consequence of the inverted positions of the substitutions, the corresponding R<sub>1</sub> brominated (e.g., the analogue of **7** and

**11**) and **R<sub>3</sub>** aminophenyl (e.g., the analogue of **9** and **13**) derivatives of **17** and **19**, respectively, should be synthesized and tested.

Furthermore, compound **15** (Series III, **R<sub>1</sub>** = fluorophenoxy, **R<sub>2</sub>** = phenyl, **R<sub>3</sub>** = H, EC<sub>50</sub> = 5 μM) shows that the inclusion of a fluorine atom on the phenyl group at the **R<sub>1</sub>** position slightly decreases the activity compared to the non-fluorinated (**12**, EC<sub>50</sub> = 1.8 μM) or the methoxy-substituted (**14**, EC<sub>50</sub> = 1.8 μM) analogues.

### 2.3. Quinones selectivity towards trypanosomatids

Next, the biological selectivity of the quinones was assessed by testing their cytotoxicity against murine macrophages. Macrophages were selected as mammalian cell model because they play an important immunological role in controlling *Trypanosoma* infection and are the host cells colonized by *Leishmania* and *T. cruzi* parasites. We performed an initial screening at fixed compound concentrations (10 μM or 50 μM) and subsequently, determined the cytotoxic concentration 50 (CC<sub>50</sub>) for those that did not impair macrophage viability to a significant extent when tested at 50 μM.

For highly cytotoxic compounds (cell viability ≤50% at 10 or 50 μM), an approximation to the CC<sub>50</sub> value is reported (Table 1). In all cases, cells were treated 24 h with the quinones. The preliminary screenings indicate that seven of them (**10**, **12**, **13**, **15**, **16**, **17** and **19**) showed a marked cytotoxicity causing a loss of viability higher than 50% at a concentration of 10 μM. Of them, **9** (5% viability) and **19** (0.5% viability) turned out to be the most cytotoxic. Seven quinones showed CC<sub>50</sub> ≤ 50 μM (**1–5**, **8** and **18**). Five quinones (**6**, **7**, **9**, **11** and **14**) had CC<sub>50</sub> ≥ 50 μM, being **6** (CC<sub>50</sub> = 118 μM) and **14** (CC<sub>50</sub> = 78 μM) the least cytotoxic.

Overall, these assays revealed a degree of cytotoxicity that paralleled the chemical nature of the quinones. For instance, the oxazolequinones stand out for being highly cytotoxic (**19** > **15** > **17** > **16**) most of them reducing macrophage viability to less than 20% at 10 μM. The naphthoquinones series included molecules with moderate (**1**, **4** and **5** CC<sub>50</sub> ~ 50 μM) to higher cytotoxicity (**2** and **3** CC<sub>50</sub> < 50 μM), whereas the thiazolequinones series contained analogues highly cytotoxic (**9** > **13** > **12** > **10**; e.g., cell viability 5–40% at 10 μM) and two derivatives with moderate and similar cytotoxicity (**11** and **14**, CC<sub>50</sub> = 61 and 78 μM, respectively). Except for **8** (CC<sub>50</sub> = 37 μM), the furanequinones contained analogues with low (**6** CC<sub>50</sub> = 118 μM) to moderate cytotoxic activity (**7** and **9**, CC<sub>50</sub> = 59 and 57 μM, respectively). For comparison, nifurtimox has a CC<sub>50</sub> = 100 μM. Comparison of the cytotoxicity of the warheads from each series (**5**, **6**, **10** and **16**) reveals that the oxazole (**16**) and thiazole (**10**) rings contribute to increase quinones cytotoxicity, whereas the naphthalene (**5**) and, to a major extent, the furane (**6**) rings exert the opposite effect.

At variance with the behavior observed against bloodstream trypanosomes, the contribution of the substitutions to macrophage cytotoxicity is heterogeneous along the series and clearly depends on the quinone scaffold context. For the furanequinones, the addition of an aryloxy fragment at C-2 increases cytotoxicity (**8** CC<sub>50</sub> = 37 μM) when compared to the unsubstituted analogue (**6** CC<sub>50</sub> = 118 μM). For Series III, the inclusion of a bromine atom at **R<sub>1</sub>** (**11** CC<sub>50</sub> = 61 μM) or methoxy-phenol group in the aryloxy fragment (**14** CC<sub>50</sub> = 78 μM) lowered significantly (>6-folds) the cytotoxicity of these analogues with respect to the unsubstituted scaffold (**10** CC<sub>50</sub> < 10 μM). For the oxazole derivatives, the inclusion of a phenol ring at **R<sub>1</sub>** (**18** CC<sub>50</sub> = 46 μM) significantly reduced the cytotoxicity with respect to the unsubstituted analogue (**16** CC<sub>50</sub> < 10 μM).

The selectivity index (SI) was calculated by determining the ratio of CC<sub>50</sub> macrophage versus EC<sub>50</sub> *T. brucei* (Table 1). Considering the SI of nifurtimox (SI = 19) as reference, only four quinones (**6**, **9**, **11** and **14**, SI = 40–63) displayed higher selectivity for killing bloodstream *T. brucei* than the clinical drug. Among them, only **9** was one of the two quinones with sub-micromolar activity against the pathogen (EC<sub>50</sub> = 0.9 μM), whereas **6**, **11** and **14** presented similar one-digit μM EC<sub>50</sub> (i.e., 1.5–2.7

μM). Quinones **1**, **2**, **4**, **5**, **8**, **13** and **18** displayed moderate selectivity (SI = 10–22), whereas **3**, **7**, **10**, **12**, **15**, **16**, **17** and **19** were the less selective ones (SI < 10).

Next, the pan-trypanosomatid activity of the most selective quinones towards *T. brucei* (**6**, **9**, **11** and **14**) was studied against the intracellular stage of *T. cruzi* and *L. infantum*. Thus, mammalian cells infected with these parasites were treated for 24 h with the compounds (at 10 or 20 μM, Table 1) and pathogen viability analyzed by bioluminescence. For *L. infantum*, none of the four quinones significantly affected the viability of amastigotes (e.g., **11** and **14** ~90% viability at 20 μM compound) whereas the control drugs did it (amphotericin B, EC<sub>50</sub> = 35 nM, and miltefosine, EC<sub>50</sub> = 38 μM). In contrast, the furanequinone **9** (EC<sub>50</sub> = 0.8 μM) and the thiazolequinone **14** (EC<sub>50</sub> = 1.1 μM) were capable to inhibit the intracellular proliferation of *T. cruzi* with potencies like those of nifurtimox (EC<sub>50</sub> = 0.7 μM) and benznidazole (EC<sub>50</sub> = 2.2 μM). The bromine in position **R<sub>1</sub>** and phenylamino in position **R<sub>3</sub>** appear to be important determinants of the anti-*T. cruzi* activity of **9** because the unsubstituted analogue (**6**) reduced only marginally (12%) parasite viability when tested at 10 μM. In the case of the thiazolequinone scaffold, the replacement of the methoxy-phenyl group present at **R<sub>1</sub>** in **14** by a bromine atom (**11**) decreased the anti-parasite activity (78% parasite viability at 10 μM compound).

Quinones are recognized pseudo-substrates of different cellular dehydrogenases and reductases [34,35]. Thus, it is tempting to speculate that the discrepancy between the high activity of several quinones against bloodstream (*T. brucei*) or intracellular (*T. cruzi*) trypanosomes and the null activity observed for a set of them towards *L. infantum* amastigotes may be consequence of a different metabolic repertoire between developmental stages and species. In fact, compared to *Leishmania* amastigotes (doubling time estimated in ~60 h to 12 days, for cultured or *ex vivo* amastigotes [36,37]) bloodstream *T. brucei* and *T. cruzi* amastigotes have a comparatively high replication rate (doubling time 5.5 h and 8–12 h, respectively [32,38]) that demands an important supply of energy and the dedicated enzymatic resources for it. Supporting this statement, studies conducted in different *Leishmania* species revealed a lower capacity of biosynthesis, a reduced bioenergetic level, and a strongly altered metabolism for the amastigote stage [39]. Furthermore, at variance with *L. infantum* amastigotes, which can rely on glycolysis and mitochondrial respiration for generation of ATP, the energetic metabolism of bloodstream *T. brucei* is fully dependent on glycolysis [40]. In this regard, GAPDH, an essential glycolytic enzyme for African trypanosomes [41] has been shown to be target of naphthoquinones [42]. In addition, it is also possible that, at the concentrations tested (10 and 20 μM), these quinones (which represented the less cytotoxic for macrophages) are efficiently reduced to the more stable and redox innocuous dihydroquinone form by dehydrogenases or reductases from the host cell. In consequence, the intracellular concentration of free quinone and semiquinone will be below that required to impair parasite viability.

### 2.4. p-Quinones induce a fast and remarkable intracellular oxidative milieu in bloodstream *T. b. brucei*

To get insights into the mode of action of quinones against bloodstream *T. brucei* and based on the well documented redox cycling effects of quinones in biological systems (Scheme 1), we evaluated their capacity to alter the intracellular redox homeostasis of low molecular weight thiols. For that purpose, bloodstream *T. brucei* parasites expressing a redox-sensitive green fluorescent protein (roGFP2) fused to human glutaredoxin (hGrx) were used. This redox reporter cell line allows detecting the intracellular fluctuations in the levels of oxidized and reduced glutathione and trypanothione via a non-invasive procedure [43,44]. We have previously employed this assay to address the mechanism of action of a wide diversity of chemical compounds [44–48].

Exponentially growing parasites were incubated for 1 h with the quinones added at 1 × or 2 × their EC<sub>50</sub> values and the fluorescence

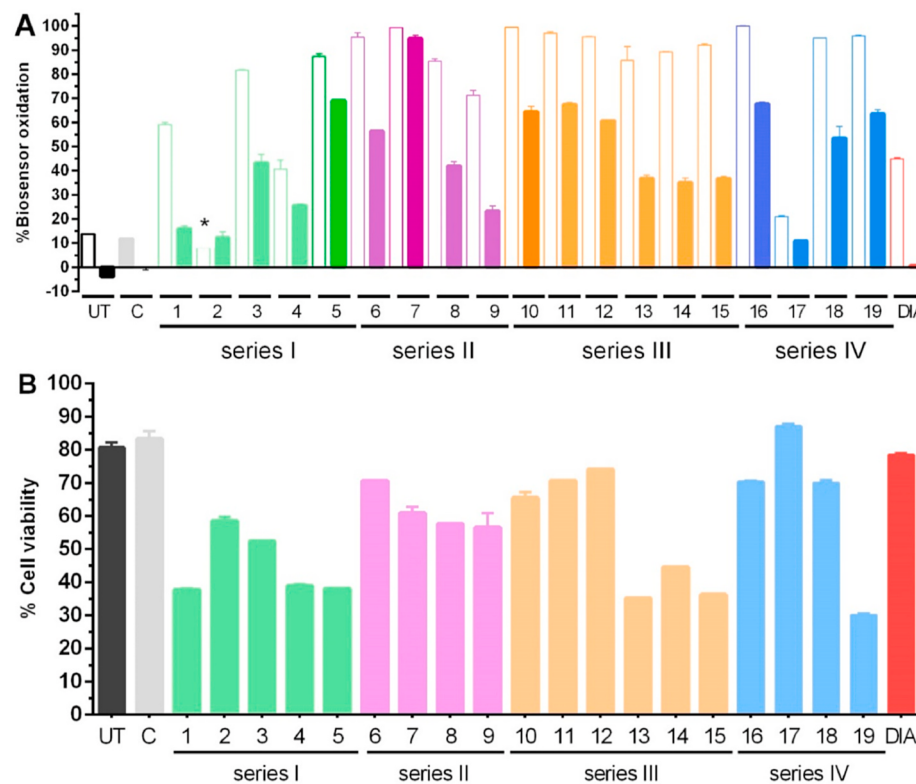


**Fig. 3. Redox activity of quinones against the infective form of *T. b. brucei*.** A) Intracellular thiol-redox balance of low molecular weight thiols determined in parasites treated with the different compounds added at 1X (3, 7–9 and 12) or 2X (1, 2, 4–6, 10, 11 and 13–19) their EC<sub>50</sub> values. Controls included parasite samples untreated (UT), treated with 1% DMSO (C) or diamide 250 µM (DIA). The color-filled bar corresponds to samples from each condition treated with DTT (1 mM). Compared to the DMSO treated control (C, grey bar), all quinones, except for compound 2 (asterisk), exerted a statistically significant oxidation of the biosensor ( $p < 0.0005$ ). B) Cell viability (expressed as %) determined in all samples by propidium iodide staining of death cells and flow cytometry analysis. The redox analysis was performed at quinones' concentrations that yielded cell viabilities  $\geq 30\%$ .

**Table 2**  
Percentage of biosensor oxidation (%BO) and DFT parameters for *p*-quinones.

Compound	%BO	$\Delta G(Q^\cdot)$	$\Delta G(QH_2)$	SUMO ( $Q^\cdot$ )	HOMO Q	LUMO Q	HOMO $QH_2$	LUMO $QH_2$
1	59.07	-404	-3345	-556.4	-706.0	-237.1	-673.1	-42.7
2	7.92*	-415	-3321	-558.1	-762.6	-249.3	-677.6	-83.3
3	81.70	-413	-3308	-554.6	-761.8	-245.9	-670.8	-35.2
4	40.54	-402	-3370	-555.6	-826.8	-237.1	-671.8	-36.8
5	87.33	-403	-3365	-556.2	-716.7	-236.9	-673.1	-44.9
6	95.33	-431	-3295	-584.0	-745.1	-261.5	-702.7	32.4
7	99.25	-445	-3290	-591.3	-749.5	-280.0	-679.6	-68.8
8	85.40	-425	-3317	-574.1	-744.3	-258.5	-657.3	-58.4
9	71.31	-423	-3283	-575.8	-709.1	-253.2	-676.9	-70.8
10	99.42	-439	-3340	-591.2	-794.2	-272.8	-715.6	-104.3
11	96.99	-453	-3290	-599.7	-797.1	-291.3	-714.9	-104.6
12	95.51	-434	-3338	-583.4	-783.5	-271.3	-705.6	-101.9
13	85.67	-431	-3283	-580.9	-724.5	-266.8	-690.6	-119.5
14	89.22	-424	-3345	-595.4	-763.3	-269.9	-697.1	-103.5
15	92.06	-436	-3307	-596.9	-789.0	-271.2	-699.6	-104.4
16	100	-445	-3357	-601.7	-795.9	-273.2	-709.3	-81.7
17	20.95	-459	-3304	-610.0	-798.7	-292.2	-732.9	-91.4
18	94.92	-439	-3344	-596.2	-789.1	-265.6	-719.4	-87.5
19	95.87	-436	-3298	-587.7	-724.6	-270.5 <sup>a</sup>	-698.4	-93.1

<sup>a</sup> Data obtained at 2X EC50.

intensity of the redox biosensor was analyzed for viable cells by flow cytometry and plotted as % biosensor oxidation (Fig. 3 and Table 2).

Despite a few exceptions highlighted below, overall, the magnitude of the oxidative milieu generated by quinones at intracellular level displayed the following increasing order: naphtho < furane < oxazole ≈ thiazole quinones. For the naphthoquinones, 1, 3 and 5 induced a significant oxidation of the biosensor (60–80%), whereas 4 did it to a comparatively lower extent (40%) and, notably, 2 did not. All the furanequinones proved to be highly pro-oxidative (70–100% biosensor oxidation) in the following order: 7 > 6 > 8 ≈ 9. Without exceptions, all thiazolequinones caused a significant oxidation of the biosensor (>80%) with 10 > 11 > 12 > 13 ≈ 14 ≈ 15. With respect to the oxazolequinones, except for 17, which produced a marginal oxidation of the

biosensor (9%), 16, 18 and 19 led to 100–80% biosensor oxidation.

It is worth noting that the redox basis of the changes in biosensor fluorescence was verified by post-treatment of quinone-exposed parasites with the membrane permeable thiol-reducing agent DTT (1 mM). In all cases, upon this procedure, the oxidation of the biosensor (and hence its fluorescence intensity) could be reverted to a great extent. Interestingly, the oxidative capacity of most quinones, except for 2, 4 and 17, was superior to that induced by a 15 min exposure to 250 µM of the thiol-oxidizing agent diamide. This clearly indicates that there is a redox component in the mode of *T. brucei* death caused by these quinones. On the other hand, the results allow to rule out the generation of intracellular low molecular weight thiol-redox unbalance as primary mechanism of action for 2, 4 and 17.

Two interesting facts emerge from these experiments: not all quinones of Series II and IV exert an oxidizing effect, and the magnitude of the oxidation does not necessarily correlate with the potency of the compound. For example, quinones substituted at  $\text{R}_1$  by a quinoloxo- (2) or hydroxy-naphthoxy fragment (4) did not show a notable redox activity despite presenting EC<sub>50</sub> values (3.8 and 5.5  $\mu\text{M}$ ) very similar to those of analogues of the same series that proved highly oxidizing for trypanosomes (1, 3 and 5: EC<sub>50</sub> = 5.2, 5.5 and 4.6  $\mu\text{M}$ , respectively).

Something similar occurs with compound 17, which is halogenated at the quinone ring. This compound has the lowest EC<sub>50</sub> value of this series (1.6  $\mu\text{M}$ ) but does not induce oxidation of the biosensor as the rest of its analogues does (16, 18 and 19) and with whom it shares an almost identical or lower trypanosomicidal activity (EC<sub>50</sub> = 2.3, 3.3 and 1.9  $\mu\text{M}$ , respectively). In the case of Series II, compounds 6 and 7 (EC<sub>50</sub> = 3.7 and 38  $\mu\text{M}$ , respectively), which lack aryloxy substitutions on the quinone ring, produced a higher level of biosensor oxidation than the more potent quinone 9 (EC<sub>50</sub> = 0.9  $\mu\text{M}$ ). Similarly, for Series III, the substitution of thiazolequinone with bromine and, to a greater extent, aryl groups was detrimental to its oxidizing activity, since the parent molecule (unsubstituted, 10) showed a slightly higher oxidizing power than the rest of the modified analogues (12–15), despite presenting similar or lower EC<sub>50</sub>s.

## 2.5. Quantitative analysis and integration of biological data and quinones' chemical and biophysical properties

The quinones here studied were subjected to *in silico* multiparametric analysis with the aim to address one major question of this study: can the bioactivity of the quinones be associated to the electronic configuration of their redox reactivity?

DFT calculations on all quinones allowed us to select a set of electronic descriptors (Table 2): the Gibbs energy of formation of the semiquinone radical from oxidized quinone as well as the energy of the frontier orbitals of several involved electronic states and their respective charges. Mulliken charges on atoms shown in Fig. 4 were successively considered as putative descriptors for QSAR.

All  $\Delta G$ 's, SUMO (Semi Unoccupied Molecular Orbital), HOMO (High Unoccupied Molecular Orbital) or LUMO (Low Unoccupied Molecular Orbital) values are expressed in  $\text{kJ mol}^{-1}$ . Electronic descriptors  $\Delta G \text{ Q}^\cdot$  and  $\Delta G \text{ QH}_2$  are the Gibbs free energies for the formation of semiquinone and hydroquinone from quinone, respectively. SUMO  $\text{Q}^\cdot$ , HOMO Q and LUMO Q, HOMO  $\text{QH}_2$  and LUMO  $\text{QH}_2$  are the values of frontier orbitals energies of semiquinone, neutral and hydroquinone

**Table 3**

Correlation indexes of the electronic descriptors with pEC<sub>50</sub> values and with the percentage oxidation of the biosensor (%BO). The asterisk denotes statistically significant correlations ( $p < 0.05$ ).

Index	pEC <sub>50</sub> r/rho	%OB r/rho
$\Delta G \text{ (Q}^\cdot)$	-0.52*	-0.89*
$\Delta G \text{ (QH}_2)$	0.53*	0.13
SUMO $(\text{Q}^\cdot)$	-0.48*	-0.78*
HOMO Q	0.16	-0.43
LUMO Q	-0.55*	-0.87*
HOMO $\text{QH}_2$	-0.37	-0.76*
LUMO $\text{QH}_2$	-0.63*	-0.43
$\eta$	-0.46	0.16
O1-Q	0.46	0.20
O2-Q	-0.08	0.14
C1-Q	-0.60*	-0.85*
C2-Q	-0.60*	0.43
C3-Q	0.87*	0.52*
C4-Q	-0.66*	-0.48
C5-Q	0.53*	0.49*
C6-Q	-0.23	0.17
Y7-Q	0.07	-0.35
C8-Q	0.74*	0.29
X9-Q	0.71*	0.36
O1- $\text{Q}^\cdot$	0.26	-0.13
O2- $\text{Q}^\cdot$	0.43	-0.09
C1- $\text{Q}^\cdot$	-0.50*	-0.70*
C2- $\text{Q}^\cdot$	-0.42	0.08
C3- $\text{Q}^\cdot$	0.79*	0.20
C4- $\text{Q}^\cdot$	-0.47*	-0.26
C5- $\text{Q}^\cdot$	0.48*	0.46
C6- $\text{Q}^\cdot$	-0.21	0.16
Y7- $\text{Q}^\cdot$	-0.28	-0.17
C8- $\text{Q}^\cdot$	0.48*	-0.08
X9- $\text{Q}^\cdot$	0.44	0.51*

species, respectively.

### 2.5.1. Relationships of *T. brucei* pEC<sub>50</sub> and electronic indexes

As a first observation of the electronic situation, the electron density distribution of the oxidized quinone (Q) LUMO and semiquinone radical ( $\text{Q}^\cdot$ ) SUMO orbitals is shown for the most (9) and least potent quinones (7, Fig. 4).

Following the hypothesis of a redox mechanism of action, the  $\Delta G$  values for the reduction of Q in a one- and two-electron process show moderate correlations with the activity in *T. brucei* (Table 3). For the  $\Delta G$

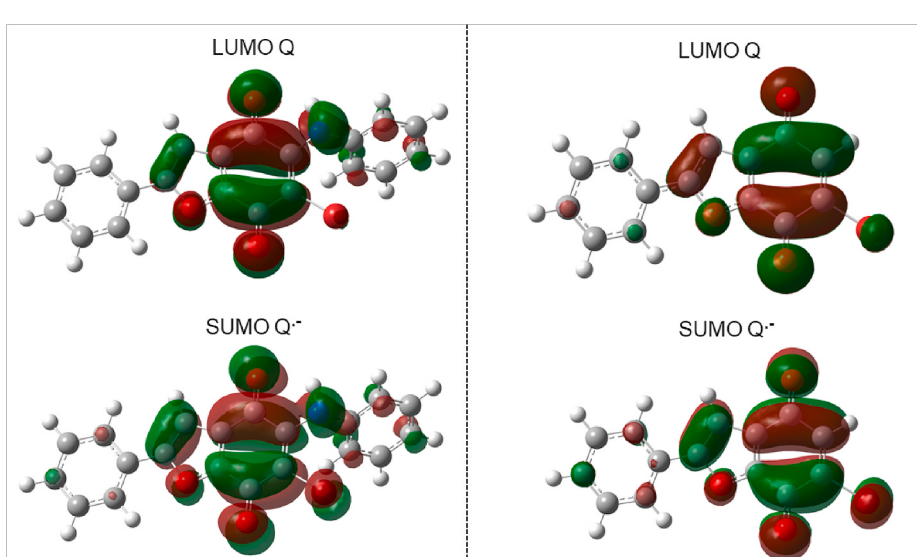


**Fig. 4.** LUMO Q and SUMO  $\text{Q}^\cdot$  frontier orbitals. Left: LUMO and SUMO orbitals for compound 9. Right: LUMO and SUMO orbitals for compound 7.

of formation of  $\text{Q}^-$ , Series I shows the lowest potency against *T. brucei* and has the highest Gibbs energy values, hence being the series with the lowest tendency to form the  $\text{Q}^-$  species (Fig. S1). There is no clear overall trend for Series II, III and IV. For the first two series, we observed that the most potent compounds against *T. brucei* (13, 9) have the highest  $\Delta G$  for the formation of  $\text{Q}^-$  of their respective series, while the other compounds show a tendency to be more potent, featuring lower  $\Delta G$ 's. Compounds 15 and 18 show a different behavior probably because of the phenoxy group in these structures, indicating that this kind of substitutions negatively affect the activity. A second index of interest is the  $\Delta G$  of formation of  $\text{QH}_2$  for which a moderate correlation is observed.

Compounds 9 and 13 show the highest  $\Delta G$  values for the formation of  $\text{QH}_2$  (Fig. S1). A third noteworthy index is the SUMO energy, for which a moderate correlation with activity in *T. brucei* is observed. Series I show higher SUMO orbital energies than the rest of the series, while being the least potent series against *T. brucei*. This may be an indicator that compounds from this series form the radical species that are most easily reduced to dehydroquinone. For Series II, III and IV there is no clear trend: compounds 15 and 18 show a lower activity compared to their series analogues and this effect may be related, as in the case of  $\Delta G$  of formation of  $\text{Q}^-$ , to the presence of the phenoxy substituent. Although to a lesser extent, a similar behavior is also observed for compound 8 (Fig. S1).

We analyzed a fourth electronic index that is the energy of the LUMO's of the oxidized species, on which the reactivity of the quinones partly depend. Overall, compounds from Series IV have highest LUMO energy and Series III, which contains a higher number of compounds with increased activity against *T. brucei*, has considerably lower LUMO energy values when compared to Series I and II. The correlation between LUMO and bioactivity is moderate for compounds from Series II and III, the exceptions being compounds 9 and 13 from each series, which have the highest LUMO energy and activity against *T. brucei*. This is interesting since this orbital receives electrons in the quinone reduction process. For Series I and IV, the most potent compounds (compounds 2 and 17) have the lowest LUMO energy values. Finally, compounds 11, 7 and 17, which have the lowest LUMO orbital energy within their series, show the same substitution pattern: a bromine atom at C3. In general, our results indicate that the compounds with the lowest LUMO energies are the most cytotoxic for *T. brucei* (Fig. S1).

The atomic charges on the benzoquinone ring show moderate and high correlations with bioactivity for both the oxidized and semiquinone species (Table 3). Charges on C1, C2 and C3 seem to be important for activity. The most potent compounds 9, 13 and 19 (second most potent in their series) have a negative charge on C2 in Q and  $\text{Q}^-$  (Fig. S1). Interestingly, these compounds have a phenylamino substituent at this position, indicating a key effect of this group on the C2 charge and suggesting that Electron Donor Groups (EDG) such as the amino group, are potentially favorable at this position. A positive charge on C3 in Q and  $\text{Q}^-$  (Fig. S1) also appears to favor activity as observed for the highly active brominated compounds 9 and 11 and the less active and negatively charged compounds from Series I. The highly electronegative properties of the bromine, i.e., electron withdrawing group at position R1 contributes to deactivate the vicinal quinone aromatic ring and confer a positive charge to C3. Yet, the substitution on C2 is shown to be more important for activity against *T. brucei* than the C3 position. This is due to the activating nature of the amine at C2 and the weak deactivating nature of bromine at C3. Finally, also the charge at C8 seems to be moderately related to activity. Although within Series II, III and IV a clear trend between charge at C8 and bioactivity was not observed, it is evident that the inclusion of this type of heteroatoms was overall favorable for quinones activity.

#### 2.5.2. Relationships between pro-oxidant activity and electronic indexes of *p*-quinones

The analysis of the intracellular oxidative power of the *p*-quinones and their electronic indexes (Table 3) revealed interesting correlations

that were also related to bioactivity against *T. brucei*. One of the most outstanding within the hypothesis of a redox mechanism is the  $\Delta G$  for the formation of  $\text{Q}^-$ . For Series I, the C3 naphthyl-substituted compounds 1 and 4 were the less oxidizing and have a large  $\Delta G$ . In contrast, the C3 phenyl-substituted analogue 3 proved more oxidizing and displayed a lower  $\Delta G$ . Compound 2, which contains a modified naphthyl ring at C3, was also less oxidizing than the phenyl-substituted analogues, suggesting that the nature of the aromatic substituent in this position is an important determinant of quinone redox activity (Fig. S2). For Series II-IV, the oxidizing potential of the compound correlated positively with more negative  $\Delta G$  values. For the  $\text{Q}^-$  SUMO and Q LUMO energies, a similar trend is observed for Series I when the analysis is carried out as a function of substitutions. For the other series, there is a correlation between higher oxidizing potential and lower  $\text{Q}^-$  SUMO and Q LUMO energies (Fig. S2).

In the case of the atomic charges, a positive correlation between oxidizing potential and negative charge at C1 (for both the Q and  $\text{Q}^-$  states) was observed. The C3 charge in Q shows a moderate correlation with respect to the oxidative capacity of the compounds: the more positive the charge, the more oxidizing the molecules tend to be. This can be exemplified by comparing compounds 7 and 9 (Series II) with compounds 11 and 13 (Series III). All four compounds are brominated at position R3, which confers C3 a positive charge. However, the phenylamino group present in R1 of 9 and 13 introduces a negative charge on C2, which counteracts the charge effect on C3 and makes these compounds less oxidizing than their R1-unsubstituted counterparts 7 and 11.

Other charges that show correlation with the oxidizing capacity of the compounds are located on C5 in Q and X9 in  $\text{Q}^-$ .

#### 2.5.3. Quantitative relationships (2D-QSAR) for $p\text{EC}_{50}$ and oxidizing potential

The normalized 2D-QSAR linear model for the  $p\text{EC}_{50}$ , obtained dividing the coefficients by the standard deviation of the variables ( $\Delta G$  of formation of  $\text{Q}^-$ , C1 charge in  $\text{Q}^-$  and C2 charge in Q), is shown in Equation (1). The number of analyzed samples was  $n = 18$  and the statistical parameters of the model yielded  $p$  value =  $1 \times 10^{-5}$ , F value = 39,  $R^2 = 0.89$  (or 0.82 applying a cross validation procedure) and RMSE = 0.09 (or 0.12 applying a leave one out cross validation procedure) [49]. The resulting parameters are above the cut-off values that define a good model (e.g.,  $R^2 > 0.6$  and low RMSE) [50,51].

$$p\text{EC}_{50} \text{ } T. brucei = -5.9439 - 0.1492 * \Delta G (\text{Q}^-) - 0.6555 * \mathbf{C1} \text{ } \mathbf{Q}^- - 0.8227 * \mathbf{C2} \text{ } \mathbf{Q} \quad (1)$$

The QSAR equation indicates that values of  $\Delta G$  for the formation of  $\text{Q}^-$  and charge on the negative atoms C1 in  $\text{Q}^-$  and C2 in Q favor activity (Fig. 5), which is consistent with the analysis made in the previous section for  $\Delta G$  for the formation of  $\text{Q}^-$  and for C2 in Q and shown in Fig. S1 for C1 in  $\text{Q}^-$ .

The normalized 2D-QSAR linear model for the level of biosensor oxidation (expressed in %), obtained dividing the coefficients by the standard deviation of the variables, is displayed in Equation (2). The number of analyzed samples was  $n = 17$  and the statistical parameters of the model were:  $p$  value =  $1 \times 10^{-5}$ , F value = 21.5,  $R^2 = 0.83$  (or 0.70 applying a leave one out cross validation procedure) and RMSE = 6.36 (or 8.52 applying a cross validation procedure). All these values are above the cut-off values that define a good model (e.g.,  $R^2 > 0.6$  and low RMSE).

$$\% \text{BO} = -9.3040 + 0.6822 * \mathbf{C2} \text{ } \mathbf{Q}^- + 0.8430 * \mathbf{C3} \text{ } \mathbf{Q} - 0.3675 * \mathbf{O1} \text{ } \mathbf{Q}^- \quad (2)$$

The QSAR equation for the oxidation of the biosensor indicates that positive charges on C2 in  $\text{Q}^-$  and on C3 of Q are favorable for activity (Fig. 6). This is consistent with the analysis performed in the previous section for C3 of Q and with Fig. S2 for C2 in  $\text{Q}^-$ . It also shows that molecules 9 and 13, which are the most active of their respective series, are the less oxidants, reinforcing the hypothesis that the phenylamino

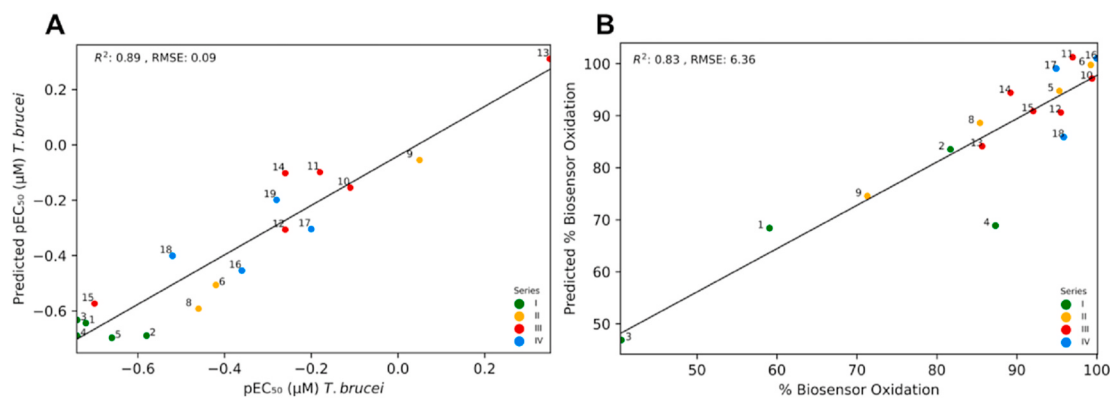


**Fig. 5.** Correlation plots for 2D-QSAR model vs experimental data. A) pEC<sub>50</sub>. B) Biosensor oxidation (%). Top left box: correlation coefficient ( $R^2$ ) of predicted vs experimental measurements and Root Mean Square Error (RMSE).

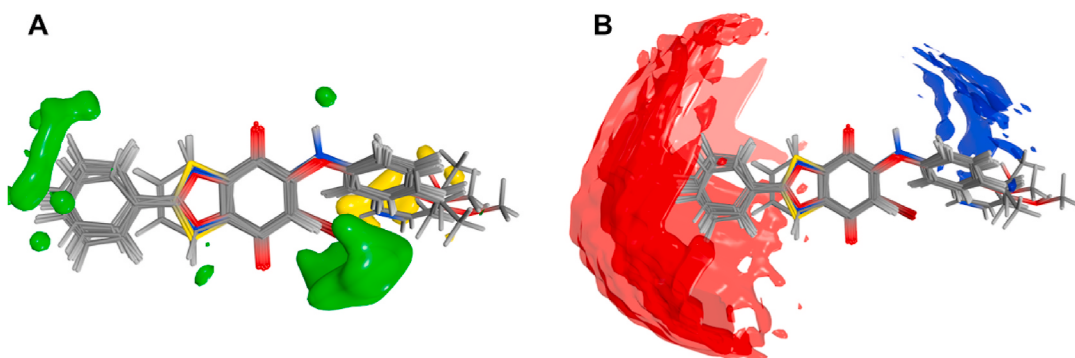


**Fig. 6.** Steric and electrostatic contour maps for all compounds. A) Yellow contours: regions where bulky substituents would decrease the activity against *T. brucei*; green contours: regions where the steric bulky groups would be favorable. B) Electrostatic contour maps. Blue contours: regions where neutral or positive charges are favorable to the activity; red regions: negative charged substituents correlate with anti-*T. brucei* activity.

**Table 4**  
Statistic parameters of the QSAR CoMFA model.

PC	RMSE	$q^2$
0	0.299	-0.121
1	0.195	0.524
2	0.155	0.701
3	0.151	0.713
4	0.160	0.679
5	0.162	0.671

substituent at C2 reduces the oxidizing capacity of the *p*-quinone and shields the electron withdrawing effect of the bromine atoms at C3.

#### 2.5.4. Three dimensional quantitative relationships with *T. brucei* activity (3D-QSAR)

The statistical parameters of 3D-QSAR, reported in Table 4,  $q^2 > 0.5$ , indicate a good predictive ability of the model [50,52,53] which was built with three principal components that minimize RMSE values and maximize the predictive potential of  $q^2$ .

A graphical summary of the analysis is shown in Fig. 6, where the yellow surfaces indicate that the presence of bulky steric groups in this region are unfavorable for activity in *T. brucei*. The yellow surface coincides with the naphthyl rings present in compounds from Series I. The green surface shows the areas where the bulky substituents favor activity, i.e., the phenyl group at C8 position. The analysis also highlights that, compared to the unsubstituted analogue, the presence of a bromine atom at the C3 position favors activity. Although bromine is not bulky compared to larger chemical groups, it has a considerable atomic radius. The red surfaces indicate regions where negatively charged groups are

favorable for activity, a large surface area is observed around the phenyl group close to C8 position, where the negative charge is a product of the  $\pi$  electron system polarized by the nearby heteroatoms.

#### 2.5.5. Relationships between anti-*T. cruzi* activity of *p*-quinones and electronic indexes

Analysis of the electronic properties of the four *p*-quinones tested against *T. cruzi* revealed that the two more active compounds 9 (Series II) and 14 (Series III) have LUMO energies that are comparatively higher than those corresponding to their significantly less active analogues 6 (Series II) and 11 (Series III). Like the behavior against *T. brucei*, the charges on C2 and C3, in both the Q and Q<sup>-</sup> states, seem to modulate quinone cytotoxicity towards *T. cruzi*. With respect to the incidence on charges of certain atoms of the quinone ring, it is noteworthy that the charge on C2 of compound 9 is negative due to the electron donor effect of the covalently bonded EDG phenylamino. In contrast, compound 6, which belongs to the same series, lacks substituents in that position and, hence, is positively charged. This suggests that the presence of an EDG group at C2 favors *p*-quinone activity against both *Trypanosoma* species. On the other hand, the charge on C3 is very different for 6 and 9 because of the effect of the bromine atom in compound 9 that confers this carbon a positive charge in both the Q and Q<sup>-</sup> states. In the case of compounds 11 and 14, they differ in the C3 substituent. The methyl phenoxy group in compound 14, being an EDG, induces a negative charge at C3 that favors activity. In contrast, the opposite electronic nature of the bromine atom (belonging to the electron withdrawing group) in the same position of 11 is detrimental for *T. cruzi* activity.

Despite the low number of compounds assayed against *T. cruzi*, this observation complies well with the results obtained for the full quinones set against *T. brucei* and validated by statistics analysis (QSAR). The

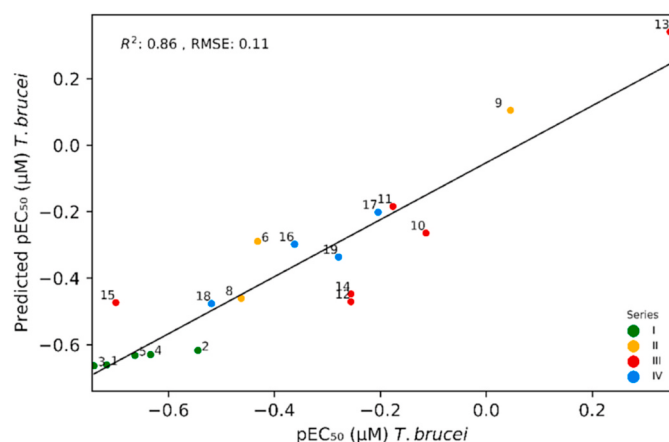


**Fig. 7.** Plot of predicted pEC<sub>50</sub> vs experimental values obtained by CoMFA. Top left box: correlation coefficient ( $R^2$ ) of predicted vs experimental measurements and Root Mean Square Error (RMSE).

relationship between predicted and measured value of pEC<sub>50</sub> are plotted in Fig. 7, whereas that obtained from the cross validation Leave One Out procedure is shown in Supplementary Material (Fig. S1)

### 3. Conclusions

Except for one molecule, all p-quinones assayed against the highly proliferative bloodstream form of African trypanosomes presented one digit to sub-μM activity. Notably, four of them have a selectivity index 2-to 3-fold higher than nifurtimox, a drug used to treat the late stage of HAT. While none of these selective quinones proved active against the intracellular stage of *L. infantum*, two of them inhibited the proliferation of the virulent strain Dm28c of *T. cruzi* with potencies in the same order of magnitude than the only two drugs in clinical use for Chagas disease. The most active and selective compounds against the extra- or intracellular infective stage of trypanosomes belong to the thiazole (Series III) and furanequinone (Series II) scaffolds, whereas the less selective ones (with respect to murine macrophages) harbor an oxazole- (Series IV) or naphthyl-scaffold (Series I).

The cytoidal effect of the compounds against *T. brucei* involved a strong pro-oxidant activity that, in a very short time, impaired the low molecular weight thiol/disulphide balance. However, not all analogues displayed a similar capacity to induce oxidative stress with certain aryloxy and halogen substitutions having a negative impact on the oxidant activity at biological level. In this regard, our working hypothesis (i.e., “the electronic configuration of the p-quinones affect their mechanism of action in trypanosomes”) was confirmed in the present study. With respect to the intrinsic properties of the p-quinones, the quantitative analysis revealed that the steric and electronic nature of the

substituents at C2 and C3 are important modulators of the anti-trypanosomal activity and oxidizing capacity of the compounds. Furthermore, there is a clear correlation (2D-QSAR) between the electronic indexes that describe the different redox states of the p-quinones and their biological reactivity. The negative of Gibbs energies of formation of the free radical anion ( $Q^-$ ) indicate that this process is thermodynamically favored. Our results also indicate that the energy of both SUMO of  $Q^-$  and LUMO, of Q are highly correlated with the observed activity. Also, the charges on C1, C2, C3 and O1 emerged as key determinants of redox reactivity displayed by the quinones. The 3D-QSAR model, which further highlighted an enhancement of p-quinone bioactivity by those bulky substituents at C3 and large negatively charged regions close to C8, supports these observations. The most important features of p-quinones revealed in this study are summarized in Fig. 8.

An additional outcome of this study was the development of QSAR models that proved robust in predicting the bioactivity and redox activity of p-quinones in *T. brucei* and, hence, can be applied to drive the development of selective candidates against this parasite species. Promising correlations were observed when the models were contrasted with the experimental data from a small subset of p-quinones tested against the related trypanosomatid *T. cruzi*. However, to confirm if the conclusions of the analysis can be extrapolated between both organisms, a larger number of quinones should be assayed in the clinically relevant stage of *T. cruzi*.

As summarized in Scheme 1, the efficient metabolism and interaction of quinones with different cellular enzymes/proteins may also contribute to their biological effects. Therefore, the remarkable differences in biosynthetic and bioenergetic capacity between bloodstream and intracellular trypanosomes (*T. brucei* and *T. cruzi*) with respect to the almost quiescent *L. infantum* amastigotes may explain the bioselectivity displayed by the p-quinones. Studies aimed to identify and experimentally validate the potential target proteins of the most potent and selective p-quinones here reported deem essential for the rational design of lead compounds.

## 4. Experimental

### 4.1. Reagents

Unless otherwise stated all chemical reagents were of analytical grade and purchased from Sigma-Aldrich or Roche. The culture media and the consumables for cell cultures were purchased from Invitrogen and Greiner, respectively. Mouse macrophage cell line J774 (ATCC® TIB-67TM) was purchased from the ATCC. The 19 quinone derivatives used in this study (Fig. 2) were synthesized according to reported proceedings [30,31].

### 4.2. Biological procedures

#### 4.2.1. Viability assays for bloodstream *T. b. brucei*

Bloodstream *T. b. brucei* (strain 427- cell line 514–1313) expressing constitutively an ectopic copy of a red-shifted luciferase gene [32] was grown in HMI-9 medium supplemented with 10% (v/v) foetal bovine serum (FBS; GIBCO®) in a humidified incubator with 5% CO<sub>2</sub> and at 37 °C. The viability assay was performed as essentially described in Ref. [32]. Briefly,  $1 \times 10^5$  parasites/ml in mid-exponential growth phase were incubated (96-well plate, 218 μL) during 24 h with quinones (2.2 μL in 100% DMSO) added at: i) a fixed concentration of 10 μM, for a primary screening, and ii) different concentrations, for determination of EC<sub>50</sub> values. Control samples included: a blank (culture medium), parasites treated with the reference drug nifurtimox or vehicle alone (1% DMSO). All samples were tested in triplicates. After 24 h incubation, 200 μL from each well were transferred to a 96-well black plate and 20 μL of a solution containing 1.5 mg/mL luciferin (prepared in PBS glucose 1% w/v) and 0.05% v/v Triton X100 was added per well. Bioluminescent signal was measured at 37 °C in a luminometer (LUMIstar OPTIMA

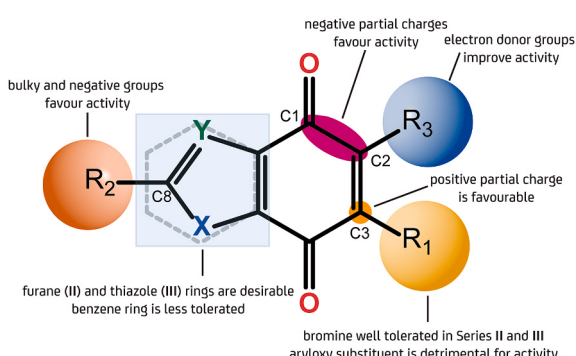


**Fig. 8.** Summary of the molecular properties of p-quinones associated with anti-trypanosomal activity.

microplate luminometer), using the following settings: 10 s shaking, 5 s/well acquisition, 0.2 s measurement delay, maximum gain, and 37 °C. Parasite viability was calculated as follows: viability (%) = 100% x [(BLS treated parasites – BLS complete media with 1% DMSO)/(BLS untreated parasites – BLS complete media with 1% DMSO)] where BLS refers to the mean of bioluminescence signal. EC<sub>50</sub> values were determined from dose-response curves fitted to a four-parameter sigmoid equation using the GraphPad Prism software (version 6.0).

#### 4.2.2. Viability assays for *L. infantum* amastigotes

*L. infantum* promastigotes from the reference strain MHOM/MA/67/ITMAP263 [54], stably transfected with a vector encoding a red-shifted luciferase gene (RE9HLUC [55]) were grown in fresh complete RPMI medium (RPMI basic medium containing 25 mM HEPES, 10% v/v FBS, 100 U/mL penicillin, 100 µg/mL streptomycin, and 15 µg/mL hygromycin B) at 28 °C in sealed culture flasks. A detailed description of the cell culture and infection/viability assay is available at [56] and is briefly outlined here. Metacyclic promastigotes were obtained by a negative selection procedure using peanut agglutinin [57] and used to infect murine macrophages (cell line J774) at a 1:10 ratio for macrophages ( $5 \times 10^6$ ): parasites ( $5 \times 10^7$ ). Two hundred µL of this suspension was added per well to a 96-well culture microplate, which was then incubated with 5% CO<sub>2</sub> at 37 °C for 24 h. Upon removing the supernatant, the cell monolayer was carefully washed with pre-warmed PBS (37 °C), prior to adding compounds 6, 9 (at 10 µM because at higher concentrations they induced macrophage detachment from the culture plate), 11 and 14 (at 20 µM), the reference drugs (amphotericin B and miltefosine) at different concentrations, or the vehicle (1% DMSO), all prepared in fresh complete RPMI medium. The culture microplate was incubated for additional 24 h. Next, the supernatant was removed, and the microplate wells were washed with pre-warmed PBS (200 µL). Luciferase activity was revealed using the Luciferase Assay System E4530 (Promega) and measured with a LUMIstar OPTIMA microplate luminometer as described in the previous section. All conditions were tested in triplicates and the percentage amastigote viability was calculated as described in section 4.2.1.

#### 4.2.3. Viability assays for *T. cruzi* amastigotes

The *T. cruzi* strain DM28c (clone TcI), stably transfected with a vector (pTRIX2-RE9h) encoding a red-shifted luciferase gene [58] was cultivated as epimastigotes in liver infusion tryptose (LIT) medium supplemented with 10% v/v FBS, 100 U/mL of penicillin, 100 µg/mL streptomycin, 40 µM of Hemin and 120 µg/mL Geneticin G418 at 28 °C.

Metacyclic trypomastigotes (MTs) were obtained by aging the epimastigotes culture (12–15 days culture with parasites in stationary phase) and further used to infect Vero cells (epithelial kidney cells from African green monkey) at a 10:1 ratio. The highly infective trypomastigotes released from the mammalian cells were then used in the screening assays described below.

Exponentially growing Vero cells were detached by trypsinisation and seeded at  $1.2 \times 10^6$  cells in fresh 5 mL of Dulbecco's Modified Eagles Medium (DMEM) supplemented with 10% FBS, 100 U/mL of penicillin, and 100 µg/mL streptomycin. After 4 h incubation (37 °C, 5% CO<sub>2</sub>), the cells were infected with  $12 \times 10^6$  *T. cruzi* trypomastigotes. After incubation for 24 h at 37 °C, 5% CO<sub>2</sub>, the cell monolayer was washed with PBS 1X and incubated with 500 µL Trypsin-EDTA (0.25%) for 5 min at 37 °C, 5% CO<sub>2</sub> to detach cells. A suspension containing infected cells ( $1.25 \times 10^5$  cells/mL) was prepared in DMEM containing 2% FBS and transferred (120 µL/well = 15000 cells/well) to a 96-well plate. The plate was incubated for 24 h at 37 °C, 5% CO<sub>2</sub> to allow differentiation from trypomastigote to amastigote. Thereafter, the medium was replaced with fresh DMEM medium + 2% FBS (120 µL/well) containing the compounds (*p*-quinones, nifurtimox or benznidazole) added at different concentrations (i.e., 10 µM for the initial screening and serial 1:3 dilutions from 20 to 0.002 µM for EC<sub>50</sub> determinations). The pathogen growth control corresponded to infected cells added of fresh

medium containing 0.5% DMSO v/v, while the inhibition control (0% growth) corresponded to wells with non-infected cells added of medium DMEM + 2% FBS with 0.5% DMSO. The culture plates were incubated for 72 h at 37 °C with 5% CO<sub>2</sub>. The luciferase activity was revealed using the Luciferase Assay System Bright Glo™ E2620 (Promega) and measured with a LUMIstar OPTIMA microplate luminometer at 25 °C as described in section 4.2.1. All concentrations were evaluated in triplicates and EC<sub>50</sub> determined as described in section 4.2.1.

#### 4.2.4. Viability assays for mouse macrophages

Murine macrophages from the cell line J774 were cultivated in a humidified 5% CO<sub>2</sub>/95% air atmosphere at 37 °C, in Dulbecco's modified Eagle's medium (DMEM) supplemented with 10% (v/v) FBS, 10 U/mL penicillin and 10 µg/mL streptomycin. Two hundred µL of a cell suspension containing  $6 \times 10^4$  cells/mL in fresh culture medium was added per well in a 96-well culture plate and incubated for 24 h. Next day, the compounds and reference drugs (nifurtimox, miltefosine or amphotericin B) were added at: i) 10 or 50 µM, for primary screening, and ii) different concentrations, for determination of EC<sub>50</sub> values. A condition with cells exposed to fresh culture medium containing 1% DMSO was included as control. The culture microplate was incubated for additional 24 h and, prior to adding the cell viability reagent (WST-1, Roche), the wells were washed with 150 µL DMEM. The microplates were incubated at 37 °C for about 2 h and absorbance at 450 nm and 630 nm was read using an EL 800-microplate reader (Biotek). The corrected absorbance values at 450 nm (Aic<sub>450nm</sub>) were obtained by subtracting the corresponding absorbance value at 630 nm and the blank average e.g., Aic<sub>450nm</sub> = Ai<sub>450nm</sub> - Ai<sub>630nm</sub> - Ablank<sub>450nm</sub>. The percentage cell viability was calculated as: % cell viability = [100% × (Aic<sub>450 nm</sub> for compound Y at concentration X/Aic<sub>450 nm</sub> in the DMSO-treated control)]. The EC<sub>50</sub> values were obtained from the corresponding concentration/response plots fitted to a four-parameter sigmoid equation or extrapolated from nonlinear fitting equations. The errors were calculated using error propagations and are expressed as S.D. estimated as σ(n-1).

#### 4.2.5. Redox assays in bloodstream *T. b. brucei*

Bloodstream *T. b. brucei* (strain 427, cell line 449) expressing the redox biosensor hGrx1-roGFP2 [53] was grown in HMI-9 medium supplemented with 10% (v/v) FBS, 0.2 µg/mL phleomycin, 5 µg/mL hygromycin, 100 U/mL penicillin/100 µg/mL streptomycin in a humidified incubator with 5% CO<sub>2</sub> and at 37 °C. At least 48 h prior to the assay, parasite growth was synchronized by inoculating  $5 \times 10^5$  cells/mL in fresh medium every 24 h and by inducing the expression of the redox reporter gene with 1 µg/mL oxytetracycline. Induced and exponentially growing parasites were harvested by centrifugation (2000 g for 10 min at room temperature) and then resuspended in PBS at a density of  $1 \times 10^6$  cells/mL. This cell suspension was added to a 96-well culture plate (198 µL/well) containing the quinones (2 µL/well) at a final concentration of 1 × or 2 × their corresponding EC<sub>50</sub> values, or the vehicle DMSO (1%). The microplates were incubated for 1 h at 37 °C with 5% CO<sub>2</sub> and then, 50 µL from each well were transferred to a new 96-well plate containing 100 µL/well of sterile PBS with glucose 1% w/v. A replicate of the samples was incubated with 1 mM DTT for 30 min (reducing condition), 250 µM diamide for 15 min (oxidizing condition) and 2 µg/mL propidium iodide (PI; exclusion dye that stains non-viable cells). All samples were analyzed with a C6 Accuri flow Cytometer (BD) with filters λ<sub>ex</sub> 488 nm/λ<sub>em</sub> 613/30 nm for PI and λ<sub>ex</sub> 488 nm/λ<sub>em</sub> 530/40 nm for GFP. The acquisition conditions were 10000 events at a medium rate of 35 µL/min. Non-viable cells (PI positive) were excluded from the redox (GFP signal) analysis and the mean fluorescence intensity (MFI) was analyzed only for samples presenting >30% viable cells (PI negative). The data were processed and analyzed with the C6Accuri and GraphPad Prism 7.00 software. The intracellular redox state (expressed as % oxidation of the biosensor) was calculated from the MFI of the biosensor normalized against diamide treatment

(MFI corresponding to 100% biosensor oxidation) and DTT treatment (MFI corresponding to 0% biosensor oxidation).

Worth noting, a short exposure time of the cells to the compounds was chosen because it allows performing an early diagnosis of the intracellular redox state of low molecular weight thiols and avoiding the potential miss-interpretation of low fluorescence intensity signals due to secondary (e.g. impaired expression, spontaneous oxidation or low chromophore maturation of the biosensor) and not to the primary effects of quinones (e.g. enzyme-mediated redox cycling activity that consumes NAD(P)H, O<sub>2</sub> and reduced thiols, and generates H<sub>2</sub>O<sub>2</sub> and radicals; Scheme 1).

#### 4.3. In silico procedures

The general *in silico* procedure consisted in building a database, modelling and optimizing the geometry of 19 3D quinone structures by means of the MMFF94x force field with the MOE program [59]. In a second step, the electronic reactivity indexes were calculated for all neutral (Q), free radical semiquinones (Q<sup>·</sup>) and hydroquinone (QH<sub>2</sub>) electronic configurations by means of density functional theory (DFT) calculations. Gibbs free energy for the formation of the semiquinones and hydroquinone from the neutral species and frontier orbitals energies as electronic descriptors were added to the database. SAR qualitative procedure was carried out to obtain a global description of the sample related to its bioactivity. The inhibition of *T. brucei* growth (pEC<sub>50</sub>) was added to the database and defined as the “bioactivity field”. Finally, 2D-QSAR and 3D-QSAR were performed to derive a quantitative relationship with respect to the physicochemical properties.

##### 4.3.1. Density functional theory (DFT)

DFT calculations were carried out with the 6-311 + G\*\* basis set on all atoms and the M05-2X1 functional, using the implicit solvent model SMD [60]. We performed a geometry optimization for the three electronic states of each one of the 19 quinones both in gas and solvent phase (water). In total, six calculations were performed for each quinone, totaling a set of 114 evaluations. With this data, the ΔG's for the transfer of two electrons in two successive one-electron steps as described below were calculated by means of a procedure suggested by Namazian et al. [61]. The first step, which delivers the semiquinone putative bioactive moiety, is shown in Equation (3A) and Fig. 9.

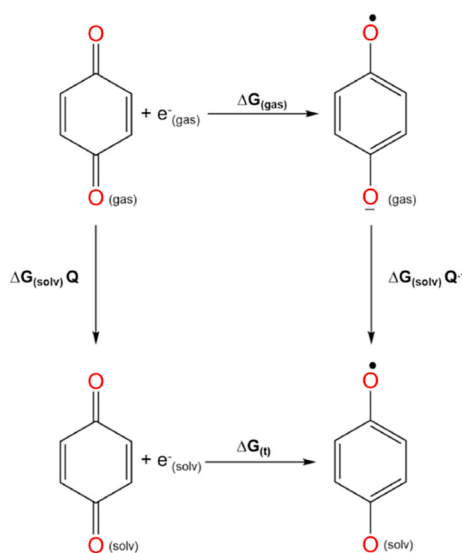
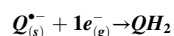


Fig. 9. Thermodynamic cycle implemented for the evaluation of electronic reduction ΔG resulting in a free radical semiquinone Q<sup>·</sup>(t).



The thermodynamic cycle used for calculating the ΔG's is shown in Fig. 9.

Many global indexes derived from the DFT calculations were evaluated for the three electronic configurations (Q, Q<sup>·</sup>, QH<sub>2</sub>) the frontier orbitals energies High Unoccupied Molecular Orbital (HOMO) and Lowest Unoccupied Molecular Orbital (LUMO) for Q and QH<sub>2</sub> states and the Semi Unoccupied Molecular Orbital (SUMO) for the Q<sup>·</sup>. Using the results of the DFT calculations, global indexes hardness ( $\eta = -1/2 (E_{\text{HOMO}} - E_{\text{LUMO}})$ ) and electronegativity ( $\chi = -1/2 (E_{\text{HOMO}} + E_{\text{LUMO}})$ ) were calculated according to Koopman's theorem.

The evaluation of Gibbs free energy for the thermodynamic cycle was made as described in Equation (4).

$$\Delta G^{\circ}_t = \Delta G^{\circ}_{(g)} + \Delta G^{\circ}(Q_{\text{Sol}}^-) - \Delta G^{\circ}(Q_{\text{Solv}}) \quad (4)$$

##### 4.3.2. Correlation of pEC<sub>50</sub> and %BO with electronic indexes

Correlation of the pEC<sub>50</sub> (-log EC<sub>50</sub>) and the percentage oxidation of the redox biosensor with the electronic indexes was performed. For the correlation, the Shapiro-Wilk test was performed on the data set of each index to determine if they corresponded to normal distributions, based on the result of this test, the corresponding regression model was applied. Pearson correlations (r) were calculated for normal distributions and Spearman correlations (rho) for non-normal distributions (see Supplementary Material Table S1 and Table S2).

For the correlation with pEC<sub>50</sub>, compound 7 (EC<sub>50</sub> = 38, Z-value = 4) was considered as outlier (Fig. S3). For the percentage oxidation of the biosensor, compounds 2 (%BO = 7.92, Z-value = 3.4) and 17 (%BO = 20.95, Z-value = 2.8) were considered as outliers (Fig. S4). The Z-values were taken with a 95% confidence interval and were therefore excluded for the construction of the statistical models.

##### 4.3.3. Structure-activity relationships (SAR)

The SAR strategy was developed by means of MOE software capacities. Following the basic SAR methodology, we performed an alignment of the molecules followed by the detection of common scaffolds, then evaluation and grouping of the substituent groups and finally wrote the report (and obtained an HTML file, available upon request) [62].

##### 4.3.4. 2D-QSAR methodology

The 2D-QSAR was carried out with the AutoSAR, svl script for MOE (AutoQSAR, MOLSIIS inc, 2020). To build the AutoQSAR model, data preparation was performed manually. AutoQSAR automatically calculates and evaluates the descriptors and eliminates unnecessary ones (correlations linearly). The following set of steps is repeated in a loop: 1) Construction of the QSAR model. 2) Cross-validation of this model. 3) Exclusion of descriptors that do not contribute to the model. Once the set of descriptors has been refined and the model has been built, the model is verified (e.g., graphically) by correlating the predicted and experimental values. This step is performed to eliminate outliers and, if necessary, to re-evaluate the model. A Cross Validation and Leave One Out (LOO) statistical analysis was applied. The output is a set of equations, annotated by their R<sup>2</sup>, RMSD and other parameters with which we selected the best QSAR-2D equation. The Z score was evaluated and a limit of Z ≥ 2.5 was applied and all data exceeding that limit were considered as outliers.

##### 4.3.5. 3D-QSAR methodology

Comparative molecular field analysis (CoMFA) in Open3DQsar software [63] was performed to study the correlation between the anti-*T. brucei* activity of *p*-quinones and their steric and electrostatic potentials [64]. First, a minimized-pose conformation of compounds was adopted, and a rigid-body alignment of molecules was performed

[65,66]. In the 3D-QSAR study a Partial Least Square (PLS) method was used for the model building, and the resulting model was validated with the LOO method for its predictive ability [49]. LOO cross-validation was used as an internal validation to determinate the principal components (PC) with the lowest RMSE ([Equation \(5\)](#)) and the highest cross-validated coefficient ( $q^2$ , [Equation \(6\)](#)).

$$RMSE = \sqrt{\frac{\sum_i (y_i - \hat{y}_i)^2}{n}} \quad (5)$$

$$q^2 = 1 - \frac{\sum_i (y_i - \hat{y}_i)^2}{\sum_i (y_i - \bar{y})^2} \quad (6)$$

Whereas  $y_i$  is the experimental EC<sub>50</sub> value of  $i$  compound,  $\hat{y}_i$  is the predicted EC<sub>50</sub> value of  $i$  compound,  $\bar{y}$  is the experimental media of the EC<sub>50</sub> values of all evaluated compounds [49,50,66].

## Author contributions

Conceptualization, M.P., M.A.C., G.P.M.; Formal analysis, C.Q., C.O., D.B., M.A.C.; Investigation (wet and *in silico* measurements): A.C.B., P.A. D., C.Q., D.F., C.O.; Organic synthesis: C.O.S., R.T., J. B., P.S.; Writing—original draft preparation: A.C.B., G.P.M., M.P., M.A.C.; Writing—review and editing: M.A.C., G.P.M., C.O.S., R.T., M.P.; Supervision: M.A.C., G.P.M., M.P.; Funding acquisition: M.A.C., M.P., C.P.M.

All authors have read and agreed to the published version of the manuscript.

## Declaration of competing interest

The authors declare not competing interest.

## Data availability

Data will be made available on request.

## Acknowledgements

M.A.C. acknowledges the support of FOCEM (Fondo para la Convergencia Estructural del Mercosur), [grant number COF 03/11]. M.P. and A.C.B. acknowledge the support of UdelaR-CSIC I + D and PEDE-CIBA programs.

## Appendix A. Supplementary data

Supplementary data to this article can be found online at <https://doi.org/10.1016/j.ejmech.2022.114926>.

## Reference

- [1] J.L. Bolton, T. Dunlap, Formation and biological targets of quinones: cytotoxic versus cytoprotective effects, *Chem. Res. Toxicol.* 30 (2017) 13–37.
- [2] L. Zhang, G. Zhang, S. Xu, Y. Song, Recent advances of quinones as a privileged structure in drug discovery, *Eur. J. Med. Chem.* 223 (2021), 113632.
- [3] G.T. Krayz, S. Bittner, A. Dhiman, J.Y. Becker, Electrochemistry of quinones with respect to their role in biomedical chemistry, *Chem. Rec.* 21 (2021) 2332–2343.
- [4] M. Rajendran, Quinones as photosensitizer for photodynamic therapy: ROS generation, mechanism and detection methods, *Photodiagnosis Photodyn. Ther.* 13 (2016) 175–187.
- [5] J. Jentsch, W.S. Koko, I.S. Al Nasr, T.A. Khan, R. Schobert, K. Ersfeld, B. Biersack, New antiparasitic bis-naphthoquinone derivatives, *Chem. Biodivers.* 17 (2020) e1900597.
- [6] E. Ortiz-Pérez, G. Rivera, C.O. Salas, J.J. Zarate-Ramos, O.S. Trofymchuk, L. Hernandez-Soberanis, J.D. Perales-Flores, K. Vázquez, Natural and synthetic naphthoquinones as potential anti-infective agents, *Curr. Top. Med. Chem.* 21 (2021) 2046–2069.
- [7] H.Y. Qiu, P.F. Wang, H.Y. Lin, C.Y. Tang, H.L. Zhu, Y.H. Yang, Naphthoquinones: a continuing source for discovery of therapeutic antineoplastic agents, *Chem. Biol. Drug Des.* 91 (2018) 681–690.
- [8] C.F.H. Ramos-Milaré Á, J. Oyama, L.S. Murase, J.V.P. Souza, B.S. Guedes, D. Lera-Nonose, M.T. Monich, A. Brustolin, I.G. Demarchi, J.J.V. Teixeira, M.V. C. Lonardoni, The anti-Leishmania potential of bioactive compounds derived from naphthoquinones and their possible applications. A systematic review of animal studies, *Parasitol. Res.* 121 (2022) 1247–1280.
- [9] L. Dantas-Pereira, E.F. Cunha-Junior, V.V. Andrade-Neto, J.F. Bower, G.A. M. Jardim, E.N. da Silva Júnior, E.C. Torres-Santos, R.F.S. Menna-Barreto, Naphthoquinones and derivatives for chemotherapy: perspectives and limitations of their anti-trypanosomatids activities, *Curr. Pharmaceut. Des.* 27 (2021) 1807–1824.
- [10] C.O. Salas, M. Faúndez, A. Morello, J.D. Maya, R.A. Tapia, Natural and synthetic naphthoquinones active against *Trypanosoma cruzi*: an initial step towards new drugs for chagas disease, *Curr. Med. Chem.* 18 (2011) 144–161.
- [11] 2020: a crucial year for neglected tropical diseases, *Lancet* 394 (2019) 2126.
- [12] J.M. Gao, Z.Y. Qian, G. Hide, D.H. Lai, Z.R. Lun, Z.D. Wu, Human African trypanosomiasis: the current situation in endemic regions and the risks for non-endemic regions from imported cases, *Parasitology* 147 (2020) 922–931.
- [13] J. Martín-Escalano, C. Marín, M.J. Rosales, A.D. Tsatsou, E. Medina-Carmona, R. Martín-Escalano, An updated view of the *trypanosoma cruzi* life cycle: intervention points for an effective treatment, *ACS Infect. Dis.* 8 (2022) 1107–1115.
- [14] A. Periferakis, A. Caruntu, A.T. Periferakis, A.E. Scheau, I.A. Badarau, C. Caruntu, C. Scheau, Availability, toxicology and medical significance of antimony, *Int. J. Environ. Res. Publ. Health* 19 (2022).
- [15] K.I. Kasozi, E.T. MacLeod, I. Ntulume, S.C. Welburn, An update on african trypanocide pharmaceuticals and resistance, *Front. Vet. Sci.* 9 (2022), 828111.
- [16] L.L.G. Ferreira, J. de Moraes, A.D. Andricopulo, Approaches to advance drug discovery for neglected tropical diseases, *Drug Discov. Today* 27 (2022) 2278–2287.
- [17] E. Izumi, T. Ueda-Nakamura, B.P. Dias Filho, V.F. Veiga Júnior, C.V. Nakamura, Natural products and Chagas' disease: a review of plant compounds studied for activity against *Trypanosoma cruzi*, *Nat. Prod. Rep.* 28 (2011) 809–823.
- [18] H. Hussain, I.R. Green, Lapachol and lapachone analogs: a journey of two decades of patent research(1997–2016), *Expert Opin. Ther. Pat.* 27 (2017) 1111–1121.
- [19] E.N. da Silva Júnior, G.A.M. Jardim, C. Jacob, U. Dhawa, L. Ackermann, S.L. de Castro, Synthesis of quinones with highlighted biological applications: a critical update on the strategies towards bioactive compounds with emphasis on lapachones, *Eur. J. Med. Chem.* 179 (2019) 863–915.
- [20] A.A.d.S. Naujoks, A.O. da Silva, R.d.S. Lopes, S. de Albuquerque, A. Beatriz, M. R. Marques, D.P. de Lima, Novel naphthoquinone derivatives and evaluation of their trypanocidal and leishmanicidal activities, *Org. Biomol. Chem.* 13 (2015) 428–437.
- [21] S. Bruno, E. Uliassi, M. Zaffagnini, F. Prati, C. Bergamini, R. Amorati, G. Paredi, M. Margiotta, P. Conti, M.P. Costi, M. Kaiser, A. Cavalli, R. Fato, M.L. Bolognesi, Molecular basis for covalent inhibition of glyceraldehyde-3-phosphate dehydrogenase by a 2-phenoxy-1,4-naphthoquinone small molecule, *Chem. Biol. Drug Des.* 90 (2017) 225–235.
- [22] M.L. Bolognesi, F. Lizzii, R. Perozzo, R. Brun, A. Cavalli, Synthesis of a small library of 2-phenoxy-1,4-naphthoquinone and 2-phenoxy-1,4-anthraquinone derivatives bearing anti-trypanosomal and anti-leishmanial activity, *Bioorg. Med. Chem. Lett.* 18 (2008) 2272–2276.
- [23] I. Sieveking, P. Thomas, J.C. Estévez, N. Quiñones, M.A. Cuellar, J. Villena, C. Espinosa-Bustos, A. Fierro, R.A. Tapia, J.D. Maya, R. López-Muñoz, B.K. Cassels, R.J. Estévez, C.O. Salas, 2-Phenylaminonaphthoquinones and related compounds: synthesis, trypanocidal and cytotoxic activities, *Bioorg. Med. Chem.* 22 (2014) 4609–4620.
- [24] R.A. Tapia, C.O. Salas, K. Vázquez, C. Espinosa-Bustos, J. Soto-Delgado, J. Varela, E. Birriel, H. Cerecetto, M. González, M. Paulino, *Synthesis and biological c* Bioorg. Med. Chem. Lett. 24 (2014) 3919–3922.
- [25] K. Vazquez, C. Espinosa-Bustos, J. Soto-Delgado, R.A. Tapia, J. Varela, E. Birriel, R. Segura, J. Pizarro, H. Cerecetto, M. Gonzalez, M. Paulino, C.O. Salas, New aryloxy-quinone derivatives as potential antiChagasic agents: synthesis, trypanocidal activity, electrochemical properties, pharmacophore elucidation and 3D-QSAR analysis, *RSC Adv.* 5 (2015) 65153–65166.
- [26] C. Ortíz, F. Moraca, M. Laverriere, A. Jordan, N. Hamilton, M.A. Comini, Glucose 6-phosphate dehydrogenase from trypanosomes: selectivity for steroids and chemical validation in bloodstream trypanosoma brucei, *Molecules* 26 (2021) 358.
- [27] M. Paulino, E.M. Alvareda, P.A. Denis, E.J. Barreiro, G.M. Sperandio da Silva, M. Dubin, C. Gastelli, S. Aguilera, O. Tapia, Studies of trypanocidal (inhibitory) power of naphthoquinones: evaluation of quantum chemical molecular descriptors for structure-activity relationships, *Eur. J. Med. Chem.* 43 (2008) 2238–2246.
- [28] B. Vera, K. Vazquez, C. Mascayano, R.A. Tapia, V. Espinosa, J. Soto-Delgado, C. O. Salas, M. Paulino, Structural analysis and molecular docking of trypanocidal aryloxy-quinones in trypanothione and glutathione reductases: a comparison with biochemical data, *J. Biomol. Struct. Dyn.* 35 (2017) 1785–1803.
- [29] S.R. Wilkinson, D. Horn, S.R. Prathalingam, J.M. Kelly, RNA interference identifies two hydroperoxide metabolizing enzymes that are essential to the bloodstream form of the African trypanosome, *J. Biol. Chem.* 278 (2003) 31640–31646.
- [30] M. Paulino, C. Espinosa-Bustos, J. Bertrand, D. Cabezas, J. Mella, B. Dávila, H. Cerecetto, A. Ballesteros-Casallas, C.O. Salas, Development of 3D-QSAR and pharmacophoric models to design new anti-*Trypanosoma cruzi* agents based on 2-aryloxynaphthoquinone scaffold, *SAR QSAR Environ. Res.* 33 (2022) 701–728.
- [31] P. Sánchez, C.O. Salas, S. Gallardo-Fuentes, A. Villegas, N. Veloso, J. Honores, M. Inman, M. Isaacs, R. Contreras, C.J. Moody, J. Cisterna, I. Brito, R.A. Tapia, Phenox- and phenylamino-heterocyclic quinones: synthesis and preliminary anti-pancreatic cancer activity, *Chem. Biodivers.* 19 (2022) e202101036.

- [32] D. Benítez, E. Dibello, M. Bonilla, M.A. Comini, A simple, robust, and affordable bioluminescent assay for drug discovery against infective African trypanosomes, *Drug Dev. Res.* 83 (2022) 253–263.
- [33] A. Kuemmerle, C. Schmid, S. Bernhard, V. Kande, W. Mutombo, M. Ilunga, I. Lumpungu, S. Mutanda, P. Nganzobo, D.N. Tete, M. Kisala, C. Burri, S. Blesson, O. Valverde Mordt, Effectiveness of Nifurtimox Eflornithine Combination Therapy (NECT) in T. b. gambiense second stage sleeping sickness patients in the Democratic Republic of Congo: report from a field study, *PLoS Neglected Trop. Dis.* 15 (2021), e0009903.
- [34] C. Espinosa-Bustos, M. Ortiz Pérez, A. Gonzalez-Gonzalez, A.M. Zarate, G. Rivera, J.A. Belmont-Díaz, E. Saavedra, M.A. Cuellar, K. Vázquez, C.O. Salas, New amino naphthoquinone derivatives as anti-trypanosoma cruzi agents targeting trypanothione reductase, *Pharmaceutics* 14 (2022) 1121.
- [35] Q. Gong, J. Hu, P. Wang, X. Li, X. Zhang, A comprehensive review on  $\beta$ -lapachone: mechanisms, structural modifications, and therapeutic potentials, *Eur. J. Med. Chem.* 210 (2021), 112962.
- [36] J. Kloehn, E.C. Saunders, S. O'Callaghan, M.J. Dagley, M.J. McConville, Characterization of metabolically quiescent Leishmania parasites in murine lesions using heavy water labeling, *PLoS Pathog.* 11 (2015) e1004683.
- [37] E.C. Saunders, W.W. Ng, J. Kloehn, J.M. Chambers, M. Ng, M.J. McConville, Induction of a stringent metabolic response in intracellular stages of Leishmania mexicana leads to increased dependence on mitochondrial metabolism, *PLoS Pathog.* 10 (2014), e1003888.
- [38] P.C. Dumoulin, B.A. Burleigh, Stress-induced proliferation and cell cycle plasticity of intracellular trypanosoma cruzi amastigotes, *mBio* 9 (2018).
- [39] M. Jara, M. Berg, G. Caljon, G. de Muylder, B. Cuypers, D. Castillo, I. Maes, M.d. C. Orozco, M. Vanaerschot, J.-C. Dujardin, J. Arevalo, Macromolecular biosynthetic parameters and metabolic profile in different life stages of Leishmania braziliensis: amastigotes as a functionally less active stage, *PLoS One* 12 (2017), e0180532.
- [40] P.A.M. Michels, O. Villafraz, E. Pineda, M.B. Alencar, A.J. Cáceres, A.M. Silber, F. Bringaud, Carbohydrate metabolism in trypanosomatids: new insights revealing novel complexity, diversity and species-unique features, *Exp. Parasitol.* 224 (2021), 108102.
- [41] A.J. Cáceres, P.A. Michels, V. Hannaert, Genetic validation of aldolase and glyceraldehyde-3-phosphate dehydrogenase as drug targets in Trypanosoma brucei, *Mol. Biochem. Parasitol.* 169 (2010) 50–54.
- [42] F. Belluti, E. Uliassi, G. Veronesi, C. Bergamini, M. Kaiser, R. Brun, A. Viola, R. Fato, P.A. Michels, R.L. Krauth-Siegel, A. Cavalli, M.L. Bolognesi, Toward the development of dual-targeted glyceraldehyde-3-phosphate dehydrogenase/trypanothione reductase inhibitors against *Trypanosoma brucei* and *Trypanosoma cruzi*, *ChemMedChem* 9 (2014) 371–382.
- [43] M. Gutscher, A.L. Pauleau, L. Marty, T. Brach, G.H. Wabnitz, Y. Samstag, A. J. Meyer, T.P. Dick, Real-time imaging of the intracellular glutathione redox potential, *Nat. Methods* 5 (2008) 553–559.
- [44] S. Ebersoll, M. Bogacz, L.M. Günter, T.P. Dick, R.L. Krauth-Siegel, A tryparedoxin-coupled biosensor reveals a mitochondrial trypanothione metabolism in trypanosomes, *Elife* 9 (2020).
- [45] F. Rivas, A. Medeiros, C. Quiroga, D. Benítez, M. Comini, E. Rodríguez-Arce, I. Machado, H. Cerecetto, D. Gambino, New Pd–Fe ferrocenyl antiparasitic compounds with bioactive 8-hydroxyquinoline ligands: a comparative study with their Pt–Fe analogues, *Dalton Trans.* 50 (2021) 1651–1665.
- [46] J. Franco, F. Sardi, L. Szilagyi, K.E. Kover, K. Feher, M.A. Comini, Diglycosyl diselenides alter redox homeostasis and glucose consumption of infective African trypanosomes, *Int. J. Parasitol. Drugs Drug. Resist.* 7 (2017) 303–313.
- [47] J. Franco, A. Medeiros, D. Benítez, K. Perelmuter, G. Serra, M.A. Comini, L. Scarone, In vitro activity and mode of action of distamycin analogues against African trypanosomes, *Eur. J. Med. Chem.* 126 (2017) 776–788.
- [48] C. Ortíz, F. Moraca, M. Laverriere, A. Jordan, N. Hamilton, M.A. Comini, Glucose 6-phosphate dehydrogenase from trypanosomes: selectivity for steroids and chemical validation in bloodstream trypanosoma brucei, *Molecules* 26 (2021).
- [49] P. De, S. Kar, P. Ambure, K. Roy, Prediction reliability of QSAR models: an overview of various validation tools, *Arch. Toxicol.* 96 (2022) 1279–1295.
- [50] D.L. Alexander, A. Tropsha, D.A. Winkler, Beware of R(2): simple, unambiguous assessment of the prediction accuracy of QSAR and QSPR models, *J. Chem. Inf. Model.* 55 (2015) 1316–1322.
- [51] V. Consonni, D. Ballabio, R. Todeschini, Comments on the definition of the Q2 parameter for QSAR validation, *J. Chem. Inf. Model.* 49 (2009) 1669–1678.
- [52] A. Golbraikh, A. Tropsha, Beware of q2!, *J. Mol. Graph. Model.* 20 (2002) 269–276.
- [53] A. Tropsha, P. Gramatica, V.K. Gombar, The importance of being earnest: validation is the absolute essential for successful application and interpretation of QSPR models, *QSAR Comb. Sci.* 22 (2003) 69–77.
- [54] S. Hendrickx, P.J. Guerin, G. Caljon, S.L. Croft, L. Maes, Evaluating drug resistance in visceral leishmaniasis: the challenges, *Parasitology* 145 (2018) 453–463.
- [55] B.R. Branchini, D.M. Ablamsky, A.L. Davis, T.L. Southworth, B. Butler, F. Fan, A. P. Jathoul, M.A. Pule, Red-emitting luciferases for bioluminescence reporter and imaging applications, *Anal. Biochem.* 396 (2010) 290–297.
- [56] Q.C. Benítez, D. A. Medeiros, M.A. Comini, A simple bioluminescent assay for the screening of cytotoxic molecules against the intracellular form of *Leishmania infantum*, *Methods Mol. Biol.* 2524 (2022) 127–147.
- [57] R.P.P. Soares, M.E. Macedo, C. Ropert, N.F. Gontijo, I.C. Almeida, R.T. Gazzinelli, P.F.P. Pimenta, S.J. Turco, *Leishmania chagasi*: lipophosphoglycan characterization and binding to the midgut of the sand fly vector *Lutzomyia longipalpis*, *Mol. Biochem. Parasitol.* 121 (2002) 213–224.
- [58] M.D. Lewis, A. Fortes Francisco, M.C. Taylor, H. Burrell-Saward, A.P. McLatchie, M.A. Miles, J.M. Kelly, Bioluminescence imaging of chronic *Trypanosoma cruzi* infections reveals tissue-specific parasite dynamics and heart disease in the absence of locally persistent infection, *Cell Microbiol.* 16 (2014) 1285–1300.
- [59] Molecular Operating Environment (MOE). Montréal, QC, Canada, H3A 2R7;
- [60] A.V. Marenich, J. Ho, M.L. Coote, C.J. Cramer, D.G. Truhlar, Computational electrochemistry: prediction of liquid-phase reduction potentials, *Phys. Chem. Chem. Phys.* 16 (2014) 15068–15106.
- [61] M. Namazian, M.L. Coote, Accurate calculation of absolute one-electron redox potentials of some para-quinone derivatives in acetonitrile, *J. Phys. Chem. A* 111 (2007) 7227–7232.
- [62] A.M. Clark, P. Labute, Detection and assignment of common scaffolds in project databases of lead molecules, *J. Med. Chem.* 52 (2009) 469–483.
- [63] P. Tosco, T. Balle, Open3DQSAR: a new open-source software aimed at high-throughput chemometric analysis of molecular interaction fields, *J. Mol. Model.* 17 (2011) 201–208.
- [64] R.D. Cramer, D.E. Patterson, J.D. Bunce, Comparative molecular field analysis (CoMFA). 1. Effect of shape on binding of steroids to carrier proteins, *J. Am. Chem. Soc.* 110 (1988) 5959–5967.
- [65] R. Abdizadeh, F. Hadizadeh, T. Abdizadeh, QSAR analysis of coumarin-based benzamides as histone deacetylase inhibitors using CoMFA, CoMSIA and HQSAR methods, *J. Mol. Struct.* 1199 (2020), 126961.
- [66] M.L. Sciu, M.D. Santi, J. Cantero, J.P. Colomer, M. Paulino-Zunini, M.G. Ortega, E. L. Moyano, Identification of pyrazolotriazinones as potential agents for hyperuricemia treatment by using in vitro and in silico studies, *SN Appl. Sci.* 2 (2020) 1298.